

UNCLASSIFIED

AD NUMBER

AD857522

LIMITATION CHANGES

TO:

Approved for public release; distribution is unlimited.

FROM:

Distribution authorized to U.S. Gov't. agencies and their contractors;
Administrative/Operational Use; JUN 1969. Other requests shall be referred to Air Force Flight Dynamics Lab., Wright-Patterson AFB, OH 45433.

AUTHORITY

AFFDL ltr 5 Apr 1972

THIS PAGE IS UNCLASSIFIED

AFFDL-TR-69-2

AD857522

**SOME NEW CONCEPTS IN OSCILLATORY
LIFTING SURFACE THEORY**

JOHN C. HOUBOLT

Aeronautical Research Associates of Princeton, Inc.

TECHNICAL REPORT AFFDL-TR-69-2

JUNE 1969

SEP 8 1969

This document is subject to special export controls and each transmittal to foreign governments or foreign nationals may be made only with prior approval of the Air Force Flight Dynamics Laboratory (FDTR), Wright-Patterson Air Force Base, Ohio 45433.

**AIR FORCE FLIGHT DYNAMICS LABORATORY
AIR FORCE SYSTEMS COMMAND
WRIGHT-PATTERSON AIR FORCE BASE, OHIO**

15

**SOME NEW CONCEPTS IN OSCILLATORY
LIFTING SURFACE THEORY**

JOHN C. HOUBOLT

Aeronautical Research Associates of Princeton, Inc.

This document is subject to special export controls and each transmittal to foreign governments or foreign nationals may be made only with prior approval of the Air Force Flight Dynamics Laboratory (FDTR), Wright-Patterson Air Force Base, Ohio 45433.

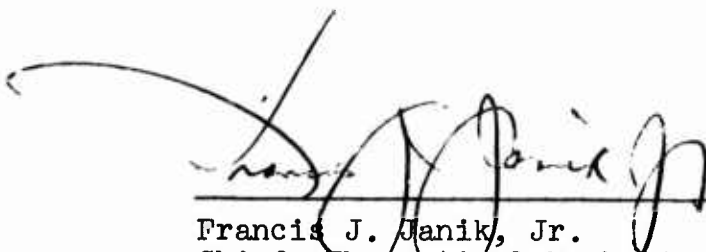
FOREWORD

This report was prepared by Aeronautical Research Associates of Princeton, Inc., Princeton, New Jersey, under Air Force Contract F33615-67-C-1191, BPSN: 7(61136702-62405334). The contract was initiated under Project No. 1367, "Structural Design Criteria," Task No. 136702, "Aerospace Vehicle Structural Loads Criteria." The work was administered under the direction of the Air Force Flight Dynamics Laboratory, Research and Technology Division, Air Force Systems Command, Wright-Patterson Air Force Base, Ohio, Mr. Paul L. Hasty (FDTR), Project Engineer.

The work reported in this study was conducted by Aeronautical Research Associates of Princeton, Inc. with Dr. John C. Houbolt as principal investigator, and covers the period 31 December 1966 to 31 October 1968. The report was submitted by the author in October 1968.

The contractor's report number is ARAP 126.

This technical report has been reviewed and is approved.



Francis J. Janik, Jr.
Chief, Theoretical Mechanics
Branch
Structures Division

ABSTRACT

New developments on lifting surface theory for oscillatory subsonic flow are given. Key concepts in the analysis are the use of concentrated loads rather than distributed pressure "mode" shapes, and the development of a modified kernel function which gives average values of vertical velocity over chosen intervals and which eliminates all singularity problems.

Features of the analysis are: (1) loads are given directly in terms of vertical velocities, (2) no pressure modes have to be assumed, (3) singularities are obviated, (4) the locations of control downwash points are specified systematically, (5) control surfaces may be included, (6) treatment of non-planar surfaces, such as T-tails, is possible, and (7) application is made through a simple quick routine procedure. Examples are given throughout to illustrate the concepts.

This abstract is subject to special export controls, and each transmittal to foreign governments or foreign nationals may be made only with prior approval of the Air Force Flight Dynamics Laboratory (FDTR), Wright-Patterson Air Force Base, Ohio 45433.

TABLE OF CONTENTS

SECTION	PAGE
I INTRODUCTION.....	1
II GOVERNING DIFFERENTIAL EQUATIONS AND BOUNDARY CONDITIONS.....	3
Governing differential equations.....	3
Boundary conditions.....	5
Basic source solutions of equations (10) and (12).	7
Point function characteristics of equations (16), (17), (18).....	8
III SOLUTION BY NUMERICAL GRIDWORK SCHEMES.....	11
Scheme I.....	12
Scheme II.....	14
Scheme III.....	16
Scheme IV.....	17
IV VERTICAL VELOCITIES FOR UNIT SOURCE ELEMENTS.....	19
Potential dipole.....	19
Unit load.....	22
V EXAMPLE SPECIFIC CASES FOR K.....	31
Case 1: 2-dimensional incompressible steady flow ($\omega = 0$).....	31
Case 2: 2-dimensional incompressible flow ($\omega \neq 0$).....	33
Case 3: 3-dimensional incompressible flow ($\omega = 0$).....	34
Case 4: 2-dimensional incompressible flow ($\omega = 0$) as derived from discrete equal loads.....	35
VI EXAMPLE TREATMENT OF WINGS.....	37
Example 1.....	37
Example 2.....	37
Example 3.....	38
Example 4.....	39
VII REMARKS ON GRID LAYOUT.....	42
VIII FREQUENCY RESPONSE AND FLUTTER DETERMINATION.....	47
By discrete masses and influence coefficients.....	47
By a modal function approach.....	49
IX CONCLUDING REMARKS.....	53
REFERENCES.....	55

ILLUSTRATIONS

FIGURE	PAGE
1. Regions of Concern and Boundary Conditions	57
2. Grid Pattern Locating Concentrated Loads and Downwash Points	57
3. Vertical Velocity Field for a Narrow Horseshoe Vortex . . .	58
4. Basic Notions of Scheme II	59
5. Establishment of "Equivalent" Concentrated Dipoles	60
6. Dipole Representation and "Averaged" Vertical Velocities .	61
7. Determination of w by Finite Difference Technique	62
8. Downwash Due to a Unit Load as Obtained from Wake Dipoles	63
9. Downwash Values for Solution 3	64
10. Downwash Solution for Unit Load by Finite - Difference Technique with z Finite	64
11. Infinite Array of Equally Spaced Concentrated Loads Replacing a Continuous Line Source	65
12. Example Airfoil Cases Treated	65
13. Ideas on Possible Grid Layouts	66

SYMBOLS

a	speed of sound
A(x)	see equation (66a)
c	chord
ci	cosine integral
i	$\sqrt{-1}$
k	reduced frequency, $k = \frac{\omega c}{2U}$
K	kernel function
\bar{K}	modified kernel function
L	lift
m	integers
M	Mach number
n	integers
p, p ₁ , p ₀ , p ⁺ , p ⁻	pressures
P	concentrated loads
Si	sine integral
t	time
u, u ₁	velocity components in the x-direction
U	steady flow velocity in the x-direction
v, v ₁	velocity components in the y-direction
w, w ₁	velocity components in the z-direction
\bar{w}	average velocity over an interval or over an area element
x, y, z	reference coordinate system
x ₀ , y ₀	coordinates to center of an area element
Z	deflection

SYMBOLS (Cont'd)

α	angle of attack; also $\alpha = e^{-\frac{i\omega\epsilon}{2U}}$
β	$\sqrt{1 - M^2}$
ϵ	interval in the x-direction
η	alternate coordinate in the y-direction
λ	interval in the y-direction
ξ	alternate coordinate in the x-direction
ρ, ρ_1, ρ_0	densities
ϕ	velocity potential
ϕ_0	strength of potential sheet
ϕ^+, ϕ^-	value of potential on upper and lower surfaces of potential sheet
ω	circular frequency

Notations:

$$\nabla^2 = \frac{\partial^2}{\partial x^2} + \frac{\partial^2}{\partial y^2} + \frac{\partial^2}{\partial z^2}$$

$l(x - x_r)$, unit step function at $x = x_r$

$\delta_y(0)$, Dirac function at $y = 0$

BLANK PAGE

SECTION I

INTRODUCTION

This report is concerned with oscillatory airforces but is motivated by the problem of determining the frequency response function of an aircraft. The frequency response function, defined in a general sense as the structural response due to a unit sinusoidal input, is now an important ingredient in the treatment of some of the major aeroelastic problems of an aircraft. Design for gusts by power spectral techniques is one area. Flutter, representing a special situation of the frequency response function, is another. Because of this prominence, a desire exists to establish the function in a quick reliable way.

The establishment of the frequency response function is conveniently broken down into two areas, one dealing with the aircraft structure, the other with the nonsteady aerodynamics. The structure is generally handled by either of two approaches, one involving the use of modal functions, the other the use of lumped or discrete masses. The aerodynamics is usually handled by modified strip theory or by a lifting surface approach involving the use of a kernel function.

In appraising the problem of determining the frequency response function, it appeared that improvements in the handling of the aerodynamics were needed. These possible improvements are discussed here mainly with reference to the use of lifting surface theory. In spite of the fact that this theory has been applied successfully in various instances, some shortcomings still exist. The approach does not seem to be as computationally economic as is strip theory (because of this fact, modified strip is still used in the treatment of very large flexible aircraft). Pressure "modes" have to be assumed from which the downwash is computed; a desire is to be able to determine the pressure directly from a prescribed downwash condition. Uncertainty still exists on how many collocation points should be used, and where they should be located. The technique for including control surfaces is not clear; only recently have some special studies of control surfaces been made. Finally, lifting surface theory has been restricted mainly to planar surfaces.

The purpose of this report is to develop improvements in the use of lifting surface theory; and, in turn, to ease the problem of determining the frequency response function. Its aims are to: (1) allow loads to be established directly in terms of given downwash values, (2) eliminate the necessity of assuming pressure modes, (3) make the choice of downwash points less arbitrary, (4) include control surfaces, (5) include nonplanar surfaces, and (6) simplify the application. Key concepts in the

development are the use of concentrated loads rather than distributed pressure mode shapes and the development of a modified kernel function which gives average values of vertical velocity over chosen intervals and which eliminates the problem of dealing with singularities.

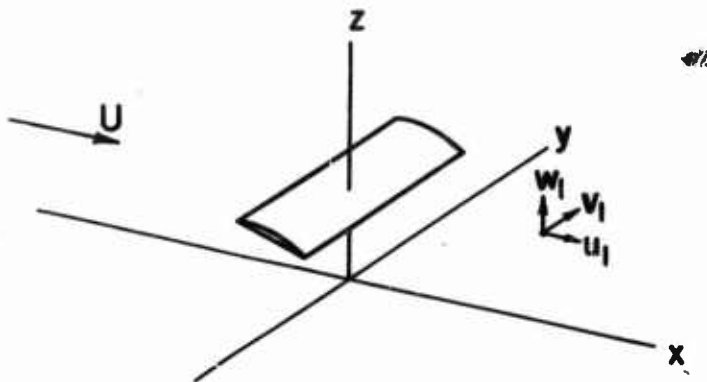
The present treatment is confined to the subsonic range, but many of the ideas should apply equally well to the supersonic range and especially in the treatment of problems involving mixed subsonic and supersonic flow.

SECTION II

GOVERNING DIFFERENTIAL EQUATIONS AND BOUNDARY CONDITIONS

Governing Differential Equations.- The developments given in this report could start directly with the well established and generally accepted linear equations for 3-dimensional oscillatory subsonic flow. For completeness, however, a brief review of their derivations is given in this section.

We consider a lifting surface immersed in a flow from the left as shown in the following sketch.



The flow is considered to be isentropic. The governing differential equations are:

Euler equations,

$$\left. \begin{aligned} \frac{\partial u_1}{\partial t} + u_1 \frac{\partial u_1}{\partial x} + v_1 \frac{\partial u_1}{\partial y} + w_1 \frac{\partial u_1}{\partial z} &= - \frac{1}{\rho_1} \frac{\partial p_1}{\partial x} \\ \frac{\partial v_1}{\partial t} + u_1 \frac{\partial v_1}{\partial x} + v_1 \frac{\partial v_1}{\partial y} + w_1 \frac{\partial v_1}{\partial z} &= - \frac{1}{\rho_1} \frac{\partial p_1}{\partial y} \\ \frac{\partial w_1}{\partial t} + u_1 \frac{\partial w_1}{\partial x} + v_1 \frac{\partial w_1}{\partial y} + w_1 \frac{\partial w_1}{\partial z} &= - \frac{1}{\rho_1} \frac{\partial p_1}{\partial z} \end{aligned} \right\} \quad (1)$$

Equation of continuity,

$$\frac{\partial}{\partial x} \rho_1 u_1 + \frac{\partial}{\partial y} \rho_1 v_1 + \frac{\partial}{\partial z} \rho_1 w_1 = - \frac{\partial \rho_1}{\partial t} \quad (2)$$

Isentropic gas law (from equation of state),

$$\frac{p_1}{\rho_1^\gamma} = c \quad (3)$$

We consider a small perturbation state by writing

$$\left. \begin{aligned} u_1 &= U + u \\ v_1 &= v \\ w_1 &= w \\ \rho_1 &= \rho_0 + \rho \\ p_1 &= p_0 + p \end{aligned} \right\} \quad (4)$$

where $u, v, w, \rho,$ and p are the perturbations which are small relative to the steady state terms. The substitution of equations (4) into equations (1), (2) and (3) yields, after discarding the second order terms, the following linearized equations

$$\left| \begin{array}{cccc} \frac{\partial}{\partial t} + U \frac{\partial}{\partial x} & & & \\ & \frac{\partial}{\partial t} + U \frac{\partial}{\partial x} & & \\ & & \frac{\partial}{\partial t} + U \frac{\partial}{\partial x} & \\ \frac{\partial}{\partial x} & \frac{\partial}{\partial y} & \frac{\partial}{\partial z} & \frac{1}{a^2 \rho_0} \left(\frac{\partial}{\partial t} + U \frac{\partial}{\partial x} \right) \end{array} \right| \begin{array}{c} u \\ v \\ w \\ p \end{array} = 0 \quad (5)$$

The speed of sound a appears in the last equation as a result of using equation (3) to replace ρ in equation (2) by p ; specifically equation (3) indicates

$$\frac{dp_1}{d\rho_1} = \frac{p}{\rho} = \gamma \frac{p_1}{\rho_1} = a^2 \quad (6)$$

The treatment of equations (5) is simplified by introducing the velocity potential ϕ such that

$$u = \frac{\partial \phi}{\partial x} \quad (7a)$$

$$v = \frac{\partial \phi}{\partial y} \quad (7b)$$

$$w = \frac{\partial \phi}{\partial z} \quad (7c)$$

With these equations all of the first three equations of equations (5) reduce identically to the equation for pressure

$$p = - \rho_0 \left(U \frac{\partial \phi}{\partial x} + \frac{\partial \phi}{\partial t} \right) \quad (8)$$

while the last equation becomes the governing differential equation

$$\nabla^2 \phi - \frac{1}{a^2} \left(U \frac{\partial}{\partial x} + \frac{\partial}{\partial t} \right)^2 \phi = 0 \quad (9)$$

Equations (8) and (9) are the basic well known equations that are to be treated in this report. It is significant to note that equations (5) show that equation (9) also applies when any of the independent variables u, v, w , or p is written in place of ϕ .

Boundary conditions.- The problem to be solved is fixed by stating the boundary conditions that must be used in conjunction with equation (9). In developing the boundary conditions it is instructive first to examine the symmetry properties of the variables u, v, w, p and ϕ . We note that the vertical velocities on the upper and lower surface of the wing must be equal (wing considered thin) and therefore reason that w must be a symmetrical function with respect to z ; equations (5) and (8) indicate then, that u, v, p and ϕ must all be anti-symmetrical with respect to z . These symmetry properties allow the flow problem to be solved by considering the upper half z -region only. Boundary conditions on the $x - y$ plane thus become of concern. It is convenient to specify these boundary conditions in terms of the three different regions A, S, and W shown in figure 1. In the region A ahead of the wing, the only perturbations that can exist are those propagated forward; no discontinuities can arise, and thus, because ϕ is anti-symmetric, $\phi = 0$ on the $x - y$ plane. For the region S, the wing supports a pressure discontinuity across its thickness

with $p^+ = -p^-$, where + and - denote respectively the upper and lower surfaces. The w in this region must be that given by the wing. The region W is established by the Kutta condition which states that w must remain finite at the trailing edge, or alternatively that $p = 0$ at this edge. From this condition it is reasoned that the wing leaves behind it a discontinuous wake sheet, which must be continuous in w , which cannot support a pressure jump, and which therefore must be discontinuous in u , v , and ϕ . Figure 1 specifies the problem completely. The main difficulty is the problem of dealing with mixed boundary conditions.

Throughout the remainder of the report we will be concerned with the oscillatory case only, where the independent variables ϕ and p may be expressed in the form

$$\phi = \phi(x, y, z) e^{i\omega t}$$

$$p = p(x, y, z) e^{i\omega t}$$

and similarly for u , v , w and ρ . Thus for the oscillatory case, equations (9) and (8) become

$$\nabla^2 \phi - \frac{1}{a^2} \left(U \frac{\partial}{\partial x} + i\omega \right)^2 \phi = 0 \quad (10)$$

$$p = -\rho_0 \left(U \frac{\partial \phi}{\partial x} + i\omega \phi \right) \quad (11)$$

The harmonic term $e^{i\omega t}$ will be suppressed for brevity in writing in all equations to follow. As mentioned earlier, equation (10) applies not only for ϕ but for the other independent variables as well; thus

$$\nabla^2 p - \frac{1}{a^2} \left(U \frac{\partial}{\partial x} + i\omega \right)^2 p = 0 \quad (12)$$

The integration of equation (11) gives a result which is basic to all subsequent development; this integration yields

$$\phi(x, y, z) = -\frac{1}{\rho_0 U} e^{-\frac{i\omega x}{U}} \int_{-\infty}^x e^{\frac{i\omega \xi}{U}} p(\xi, y, z) d\xi \quad (13)$$

Of concern also is the result obtained from this equation as $z \rightarrow 0$; this result is

$$\phi^+(x,y,0) = -\frac{1}{\rho_0 U} e^{-\frac{i\omega x}{U}} \int_{-\infty}^x e^{\frac{i\omega \xi}{U}} p^+(\xi,y,0) d\xi \quad (14)$$

where the + sign signifies values at the upper surface of the discontinuous sheets. Equations (10) through (14) form the basis for the developments in the subsequent sections. In a general sense, solutions are made by means of equations (13) or (14), in terms of basic source solutions of either equations (10) or (12), and with due regard being given to the boundary conditions.

Basic source solutions of equations (10) and (12).- Some solutions of equations (10) and (12) that form the base for the solutions of various oscillatory flow cases are the following (see reference 2):

Monopole (of unit strength),

$$\phi_m \text{ or } p_m = -\frac{1}{4\pi R} e^{-i\omega \frac{-Mx+R}{a\beta^2}} \quad (15)$$

Dipole (of unit strength),

$$\phi_d \text{ or } p_d = -\frac{\beta^2 z}{4\pi R^3} \left(1 + \frac{i\omega R}{a\beta^2}\right) e^{-i\omega \frac{-Mx+R}{a\beta^2}} \quad (16)$$

where

$$R = \sqrt{x^2 + \beta^2(y^2 + z^2)}$$

$$\beta^2 = 1 - M^2$$

These two equations are related by the operation

$$\phi_d = -\frac{\partial \phi_m}{\partial z}$$

Two other solutions that are used herein are the following reduced cases:

Line dipole for 2-dimensional incompressible flow,

$$\phi \text{ or } p = - \frac{1}{2\pi} \frac{z}{x^2 + z^2} \quad (17)$$

Dipole for 3-dimensional incompressible flow,

$$\phi \text{ or } p = - \frac{1}{4\pi} \frac{z}{R^3}, \quad R = \sqrt{x^2 + y^2 + z^2} \quad (18)$$

Point function characteristics of Eqs. (16), (17), (18).-

We remark here on the point function character of equations (16) (17) and (18), especially with respect to the use of a factor 2; some concern arises at times as to whether or not a factor 2 should be included, and these remarks are offered for possible clarification. Consider a 2-dimensional pressure discontinuity sheet extending from $x = x_1$ to $x = x_2$. The strength is specified by the function $p_0(x)$, which by the antisymmetric nature of p implies a pressure of $-1/2p_0$ on the upper surface of the sheet and $+1/2p_0$ on the lower surface. The dipole strength in an elemental length dx is $p_0(x)dx$, and thus from equation (17) the field pressure may be found as

$$p(x, z) = - \frac{1}{2\pi} \int_{x_1}^{x_2} \frac{z p_0(\xi) d\xi}{(x - \xi)^2 + z^2} \quad (19)$$

In considering this equation in the limit $z \rightarrow 0$, we note that only the portion of the integrand in the immediate vicinity of x can contribute to the integral. The equation may be reduced therefore to

$$p(x, z) = - \frac{p_0(x)}{2\pi} \int_{-\epsilon}^{\epsilon} \frac{z d\eta}{\eta^2 + z^2}$$

where the interval $\eta = -\epsilon$ to $\eta = \epsilon$ is small enough so that

$p_0(\xi)$ may be considered constant. This equation yields

$$\begin{aligned}
 p^+(x,0) &= \lim_{z \rightarrow 0} \frac{-p_0(x)}{2\pi} \tan^{-1} \frac{\eta}{z} \Big|_{-\epsilon}^{\epsilon} \\
 &= -\frac{1}{2} p_0(x)
 \end{aligned} \tag{20}$$

thus indicating the pressure to be the upper surface pressure, as it should; the point function character of equation (17) is thus also seen.

If $p_0(x)$ given by equation (20) is substituted in equation (19), we have

$$p(x,z) = \frac{1}{\pi} \int_{x_1}^{x_2} \frac{zp^+(\xi,0)d\xi}{(x-\xi)^2 + z^2} \tag{21}$$

From equations (19) and (21), we thus make the following rule: if the discontinuity strength is specified use equation (17) as is to deduce the field pressure (equation (19)); if the upper surface pressure is specified use equation (17) with the factor $-1/2$ suppressed to deduce the field pressure (equation 21)). These observations may seem trivial, but trouble has occurred in instances where they have not been fully understood.

A similar point function proof and rule may be shown to hold in the application of equations (16) and (18).

BLANK PAGE

SECTION III

SOLUTION BY NUMERICAL GRIDWORK SCHEMES

The oscillatory problem under consideration here may be stated as follows. Consider a wing to be oscillating sinusoidally in the z-direction in some prescribed deflection shape; we wish to find the particular solution of equations (10) or (12) which gives the pressure distribution on the wing and for which all the essential boundary conditions are satisfied. Such a direct solution has been possible for only a few special cases, such as 2-dimensional incompressible flow. For the more general cases solution has had to proceed in an inverse sense; thus, a pressure distribution is assumed and solution is made for the vertical velocities that are induced. To be more specific let us review the basic steps of the kernel-function approach that has been used in the past. Equation (16) for p_d is substituted into equation (13), from which the vertical velocities are found by equation (7c); formally the result appears as

$$w = K(x,y,0) = - \frac{1}{\rho_0 U} e^{-\frac{i\omega x}{U}} \lim_{z \rightarrow 0} \frac{\partial}{\partial z} \int_{-\infty}^x e^{\frac{i\omega \xi}{U}} p_d(\xi, y, z) d\xi \quad (22)$$

This function is called the kernel function; it is analogous to an influence coefficient development and specifically denotes the vertical velocity that is developed at the point $(x,y,0)$ due to a unit pressure dipole at the origin. Its evaluation and a discussion of the associated singularities are given in reference 1. With this equation the vertical velocity that results from a given loading distribution p_0 over the wing follows as

$$w = \iint_S p_0(\xi, \eta) K(x - \xi, y - \eta, 0) d\eta d\xi \quad (23)$$

To insure satisfaction of the Kutta condition, the distribution is chosen so that p_0 is zero at the trailing edge. To obtain the solution for specific lifting surfaces the technique generally used is to introduce several pressure "modes" or distributions and then by a collocation technique to find what combination of these pressure modes leads to the desired vertical velocities on the wing. In terms of the wing deflection Z , and in terms of any gust velocities w_g that also may be under consideration, these vertical velocities are given by

$$w = U \frac{\partial Z}{\partial x} + \frac{\partial Z}{\partial t} - w_g \quad (24a)$$

$$= U \frac{\partial Z}{\partial x} + i\omega Z - w_g \quad (24b)$$

where the second relation is for the sinusoidal case. It is noted that the evaluation of K and its use in equation (23) is fraught with horrible singularities.

The treatment to follow has three objectives: (1) to make a direct solution of the pressures in terms of the vertical velocities, (2) to obviate the necessity for introducing pressure "mode shapes", and (3) to greatly simplify or eliminate the problem of dealing with the difficult singularities. Four possible procedures are advanced.

Scheme I. - This scheme is based on equations (22) and (23), but with notable changes so as to allow numerical evaluation to proceed differently. The wing is divided into a gridwork pattern as shown in figure 2, guidelines for laying out this grid pattern will be brought out later. The loading on the wing is considered to be given in terms of concentrated loads rather than in terms of distributed pressure functions; this is one of the key concepts of the approach. The concentrated loads are located at the grid intersection points. Then by means of a "modified" kernel function, downwash values are derived at each mid-station point, illustrated by the point labelled A in figure 2; the logic behind the choice of the mid-station is also brought out subsequently. The result is a matrix equation which relates the loads P in terms of the downwash w . This matrix equation is then inverted, giving the desired end result of P in terms of w .

The second key point in the development of this scheme is the manner in which the kernel function is handled. The strong singularities of the kernel function along the x -axis aft of the unit load preclude its direct use in this scheme. An appreciation of the type of singularities involved can be obtained by picturing the downwash that is associated with a very narrow horseshoe vortex in incompressible flow, as shown in figure 3(a). The downwash pattern is singular in both the x and y directions at the origin, and strongly so in the y -direction along the horseshoe. The picture becomes all the more dramatic if we envision the situation as the width of the horseshoe becomes zero. To remove the difficulty of dealing with these singularities we modify the kernel function by averaging the velocities over equally spaced intervals in the y -direction, specifically we write

$$\bar{K}(x, y_0) = \frac{1}{\lambda} \int_{y_0 - \frac{\lambda}{2}}^{y_0 + \frac{\lambda}{2}} K(x, y) dy \quad (25)$$

where λ is the grid spacing in the y -direction. With this simple modification, the downwash function changes to the type illustrated in figure 3(b). Slice a typifies, for example, the downwash in the y -direction ahead of the unit load; slice b, a station x aft of the load. This averaging concept is based on the idea that in any real situation, the wing merely senses an average effect. Thus, by this averaging technique, the singularities in the y -direction are removed from further consideration. Note, a singularity remains in the x -direction at the unit load, but it does not concern us because we avoid any downwash consideration at this point (if desired, however, we can also consider an averaging out process in the x -direction to eliminate this singularity).

In terms of equation (25), we summarize this scheme in terms of a matrix equation as follows:

$$\begin{array}{c|ccc|cccc|c} w_1 & \bar{K}_{11} & \bar{K}_{12} & \bar{K}_{13} & \cdot & \cdot & \cdot & P_1 \\ w_2 & \bar{K}_{21} & \bar{K}_{22} & \bar{K}_{23} & \cdot & \cdot & \cdot & P_2 \\ w_3 & \bar{K}_{31} & \cdot & \cdot & \cdot & \cdot & \cdot & P_3 \\ \cdot & \\ \cdot & \\ \cdot & \end{array}$$

or

$$|w| = [\bar{K}]|P| \quad (26)$$

where \bar{K}_{mn} denotes simply the "average" value over the interval λ in the y -direction of the downwash at station m due to a load at station n . Inversion of equation (26) gives the desired end results.

$$|P| = [\bar{K}]^{-1} |w| \quad (27)$$

There are several noteworthy points to bring out with respect to the use of equation (26):

- (1) No load or pressure distributions have to be assumed.

- (2) It is not necessary to force any load or pressure distribution to be zero at the trailing edge (the condition of zero pressure jump across the trailing wake sheet will be satisfied automatically because this condition is satisfied for each of the concentrated loads).
- (3) The question of how many collocation points should be used, and where to locate them does not enter.
- (4) Quite significantly, this procedure affords a way for treating control surfaces as well; it is only necessary to distribute concentrated loads on the control surfaces in the same manner as on the wing, and to process these simultaneously with the wing loads.
- (5) The averaging technique eliminates, as mentioned, any difficulties with singularities.
- (6) The procedure is very routine and systematic; on evaluation and tabulation, the K values become universal; the establishment of the K matrix for any case becomes simply a procedure of look up, as in the use of trigonometry tables.
- (7) The \bar{K} matrix has certain symmetrical properties and many elements are identical. For example, $K_{mn} = K_{pq}$, where p and q have the same position relative to one another as do m and n ; also $\bar{K}_{mn} = \bar{K}_{pn}$, where m and p denote stations of equal distance to the right and to the left of n (the y -direction).
- (8) The scheme applies to any planform.

Scheme II.- In this scheme the essential building block is the dipole source rather than the kernel function, and explicit consideration is given to the wake. Steps are illustrated in figure 4 and are basically as follows. First, we divide the wing into a grid pattern as in Scheme I, and affix a system of concentrated loads. Next we apply equation (14) along each chordwise gridline to establish the strength of the associated dipole line sources for velocity potential that lie in the chord plane of the wing. These line sources are functionally continuous between the concentrated loads, and jump at each load location. We note here the reminder that with respect to equation (14), $\phi_0(x,y) = -2\phi^+(x,y,0)$, and $p_0(x,y) = -2p^+(x,y,0)$. Essentially, envision that we derive a system of dipole line sources which when operated upon by equation (11) yields back the concentrated load system in the limit $z \rightarrow 0$.

We then replace this line source distribution by a system of "equivalent" discrete dipoles, located at the mid-station points; the strength of each dipole is given by $\epsilon\phi_0(x,y)$, where ϕ_0 is the strength of the line source at the mid-station. Finally, we find the total downwash at the mid-station grid points on the wing due to all the discrete dipoles - those in the wake as well as in the wing planform. A matrix equation similar to equation (26) results which gives the downwash in terms of the concentrated loads; this equation is then inverted, as in Scheme I. The application of this sequence of thought may seem cumbersome, but in practice is quite simple and systematic.

In using equation (14) to establish the line source distribution, we treat each concentrated load in the nature of a Dirac function. For a single concentrated unit load, located a distance x_r downstream from a reference origin, the line source distribution for potential, as established by equation (14), is

$$\phi_0(x,y) = -2\phi^+(x,y,0) = -\frac{1}{\rho_0 U} e^{\frac{i\omega}{U}(x_r - x)} l(x - x_r) \quad (28)$$

where $l(x - x_r)$ denotes a unit step function at $x = x_r$. The sequence of using this equation for a row of concentrated loads and the means for establishing the system of equivalent concentrated potential dipoles is illustrated in figure 5.

Two versions for treating the downwash from the individual equivalent dipoles bear investigation. These are depicted in figure 6. In the first version we average the downwash over equally spaced intervals in the y -direction only, while in the second version an averaging is made in both the x and y direction. This averaging removes the singularity problem associated with the dipoles. These two averaging techniques are given by the following equations in terms of the potential for a dipole of unit strength.

$$\bar{w}_1(x,y_0) = \frac{1}{\lambda} \int_{y_0 - \frac{\lambda}{2}}^{y_0 + \frac{\lambda}{2}} \left. \frac{\partial \phi_d}{\partial z} \right]_{z=0} dy \quad (29)$$

$$\bar{w}_2(x_0,y_0) = \frac{1}{\epsilon\lambda} \int_{x_0 - \frac{\epsilon}{2}}^{x_0 + \frac{\epsilon}{2}} \int_{y_0 - \frac{\lambda}{2}}^{y_0 + \frac{\lambda}{2}} \left. \frac{\partial \phi_d}{\partial z} \right]_{z=0} dy dx \quad (30)$$

Examples later on will bring out the effect of averaging or not averaging in the x-direction.

It should be noted that the equation relating w and P as obtained by this method should be essentially the same as equation (26). The only difference might be that of a slight variation in the individual values of the coefficients K_{mn} , due to the use of different numerical procedures.

All the points relative to the utility of Scheme I apply to this scheme also, but some further points may be made. The fact that the wake must be considered explicitly may at first make the scheme appear unwieldy. This is really not so, however; the influence of downstream wake points decays very rapidly, and thus from a practical point of view we can ignore the wake beyond a certain number of chords distance; that is, we simply terminate the wake. An example presented later will bring out the effect of wake termination. With respect to giving explicit consideration to the wake we note also that, very significantly, we can turn this fact to our advantage. Since we have effectively established the complete system of potential dipoles for our wing system, we can calculate all of the induced velocities u, v, w , anywhere in the field as well as on the wing. This fact means that we are not restricted to planar lifting surfaces, and that the interaction effects of various other lifting surfaces in the vicinity of the wing may be handled as well. The big additional advantage that is offered by this scheme is therefore the fact that various configurations such as planar wings, wings with jumps, bi- or multi-wing configuration, T-tails, can be analyzed.

Scheme III.- This scheme represents a combination of schemes I and II. The key idea in this scheme is the recognition that the effect of entire wake may be expressed in terms of a concentrated load just off the wing at the trailing edge. This concentrated load is not part of the load on the wing, but the downwash it creates on the wing is precisely that contributed by the wake. It seems strange that this fact has not been recognized or utilized in previous analyses. We will deal only with the wake treatment in this section, since otherwise the scheme is the same as in scheme II.

We consider the situation that develops along one of the chord gridlines and especially the extension into the wake region. If we denote by m the number of concentrated loads that are chosen along a chord, then, by the process that is illustrated in figure 5, we find that the intensity per unit length of the wake line source is given by

$$\phi_0 = - \frac{1}{\rho_0 U} \left(P_1 + P_2 \alpha^{-2} + P_3 \alpha^{-4} + \dots + P_n \alpha^{-2m+2} \right) e^{\frac{i\omega}{U} (x_r - x)}$$

With reference to equation (28), this equation may be written

$$\phi_0 = - \frac{1}{\rho_0 U} P_e e^{\frac{i\omega}{U} (x_e - x)} l(x - x_e) \quad (31)$$

where

$$P_e = P_1 \alpha^{2m} + P_2 \alpha^{2m-2} + P_3 \alpha^{2m-4} + \dots + P_m \alpha^2 \quad (32)$$

$$x_e = x_r + m\epsilon \quad (33)$$

$$\alpha = e^{-\frac{i\omega\epsilon}{2U}}$$

Equation (31) is, however, precisely the line source intensity of the wake that would result from a concentrated load of magnitude P_e acting at station x_e . This concentrated load acting just off the trailing edge can therefore be used in place of the wake to deduce the downwash velocities that are due to the wake. For the case shown in figure 5, where $m = 4$, the concentrated load P_e would be located midway between ϕ_{04} and ϕ_{05} , and would replace all the wake to the right of this location. The equivalent wake load is handled by use of the kernel function as in scheme I. It is to be understood that an equivalent concentrated wake load is located at the aft end of each grid chord line, and that of course the superimposed downwash effect of all these loads must be considered.

In summary for this scheme, over the wing region we use the equivalent concentrated dipole concept of scheme II, and in place of the wake make use of the equivalent concentrated load given by equation (32). It is significant to note that we deal only with the downwash velocities ahead of this equivalent concentrated wake load in treating the wing. There are no singularities in this region, as the kernel function so indicates (except at the concentrated load, which region does not concern us) and hence a singularity problem associated with the concentrated wake forces is not involved.

Scheme IV. - We present here only a brief discussion of a 4th possible scheme. The basic idea of the scheme is to start with the strength of the potential dipole sheet that is present on the wing and in the wake, and to represent this strength

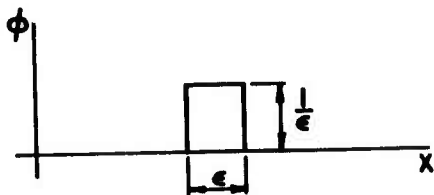
by convenient distributions, say in the form of continuous functions, step functions, or concentrated sources. The downwash and the loading would follow from this distribution by equations of the type

$$|w| = |A_1| |\phi|$$

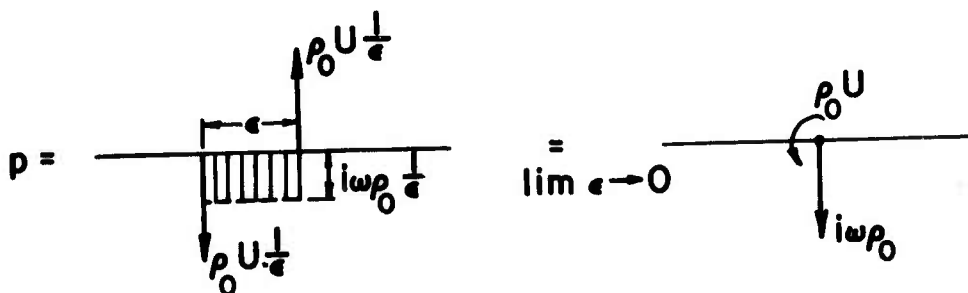
$$|P| = |A_2| |\phi|$$

The elimination of ϕ from these equations would in turn establish a relation between P and w , similar to those derived in the previous schemes.

The details of this scheme are left for further development. A derivation of the loading that is associated with a concentrated potential dipole is considered to be of interest however, and will be given here. Assume a rectangular strength distribution in the x -direction as shown in the following sketch



In the limit as $\epsilon \rightarrow 0$ this distribution becomes a concentrated dipole of unit strength. Application of equation (11) to this distribution yields the following force diagrams



Thus we see that a potential dipole of unit strength is acted upon by a force of magnitude $-i\omega\rho_0$ and a moment of magnitude $-\rho_0 U$. These results, although established here in a rather elementary way, may also be derived by a more formal approach; that is, apply equation (11) to equation (16), then determine the pressures and the moment of the pressures about the origin by integration along the entire x -axis, assuming z to be very small.

SECTION IV

VERTICAL VELOCITIES FOR UNIT SOURCE ELEMENTS

Potential dipole.- The vertical velocities in the x - y plane for unit potential dipoles, such as those given by equations(16) through (18), can be established in a very simple unconventional way by a technique described in this section. We show the method here, not so much because it eases the treatment of dipoles, but because it illustrates the technique to be used in the next section for treating unit loads, for which cases the method leads to a marked simplification over conventional approaches.

The formal way to determine the downwash due to a source potential is to use equation (7c) and then to evaluate the results for $z = 0$. We can simplify the process by expressing equation (7c) in difference form as follows

$$w = \frac{\phi(z) - \phi(0)}{z} \quad (34)$$

In all the cases of concern to us in this paper, however, $\phi(0) = 0$ for $x \neq 0$ and $y \neq 0$; thus, for all regions except at the origin, w is given simply by the potential equation with the z in the numerator removed, and with z set equal to zero elsewhere in the equation. At a glance, equations (16), (17) and (18) yield, for example:

For equation (16),

$$w = - \frac{\beta^2}{4\pi R^3} \left(1 + \frac{i\omega R}{a\beta^2} \right) e^{-i\omega \frac{-Mx+R}{a\beta^2}} \quad (35)$$

where

$$R = \sqrt{x^2 + \beta^2 y^2}$$

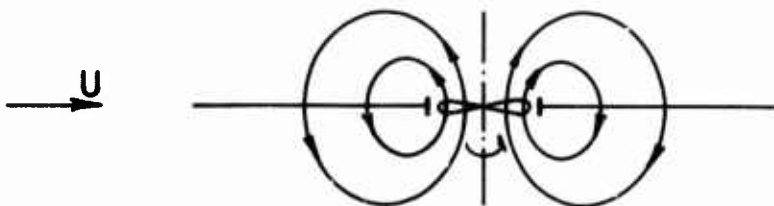
For equation (17),

$$w = - \frac{1}{2\pi} \frac{1}{x^2} \quad (36)$$

For equation (18),

$$w = -\frac{1}{4\pi} \frac{1}{(x^2 + y^2)^{3/2}} \quad (37)$$

These equations apply to all points except the origin. The flow through the origin, where a singularity is involved, is handled conveniently by use of the finite grid concept; specifically, we obviate the necessity for considering the singularity in detail by establishing the average velocity through a grid area which surrounds the origin. As an example, the central "standpipe" of the velocity profiles shown in figure 6 depicts this average velocity. In effect we have replaced the point source dipole by an equivalent dipole of finite size, very much like the propeller dipole system shown in the following sketch



The magnitude of the average velocity through the central grid area is simply the sum of velocities through all other grid areas, a fact which follows from an overall continuity condition; stated in a physical sense, we note that all the fluid that goes up must come down.

For application purposes we need to evaluate the velocity profiles for the dipoles of interest. Two will be considered here. For the case of a subsonic dipole, numerical integration of equation (35) is required. Specifically, patterned after equation (30), we write the average value of velocity over a grid area element as

$$\bar{w}_n = -\frac{\beta^2}{4\pi\epsilon\lambda} \int_{x_n - \frac{\epsilon}{2}}^{x_n + \frac{\epsilon}{2}} \int_{y_n - \frac{\lambda}{2}}^{y_n + \frac{\lambda}{2}} \frac{1}{R^3} \left(1 + \frac{i\omega R}{a\beta^2}\right) e^{-i\omega \frac{-Mx+R}{a\beta^2}} dydx \quad (38a)$$

where $R = \sqrt{x_n^2 + y_n^2}$, and where x_n and y_n denote the coordinates of the center of the grid area. From this equation we find the average velocity over the grid area surrounding the origin to be

$$\bar{w}_0 = - \sum_n \bar{w}_n \quad (38b)$$

For the case of the line dipole for 2-d incompressible flow, velocity profiles may be found by the exact integration of equation (36). The average value over an interval ϵ , having a center coordinate designated by $x_n = n\epsilon$, is

$$\begin{aligned} \bar{w}_n &= - \frac{1}{2\pi\epsilon} \int_{x_n - \frac{\epsilon}{2}}^{x_n + \frac{\epsilon}{2}} \frac{1}{x^2} dx \\ &= - \frac{2}{\pi\epsilon^2} \frac{1}{4n^2 - 1} \end{aligned} \quad (39a)$$

The center velocity \bar{w}_0 is then

$$\begin{aligned} \bar{w}_0 &= 2 \cdot \frac{2}{\pi\epsilon^2} \sum_{n=1}^{\infty} \frac{1}{4n^2 - 1} \\ &= \frac{2}{\pi\epsilon^2} \end{aligned} \quad (39b)$$

where the factor 2 accounts for the intervals to the left as well as to the right of the origin. The effect of not averaging over any of the intervals except the center interval can be demonstrated quite easily by this case. If we simply choose the velocity for an interval to be the value at the interval center, then we have

$$w_n = - \frac{1}{2\pi\epsilon^2} \frac{1}{n^2} \quad (40a)$$

$$\begin{aligned}\bar{w}_0 &= 2 \cdot \frac{1}{2\pi\epsilon^2} \sum_{n=1}^{\infty} \frac{1}{n^2} \\ &= \frac{\pi}{6\epsilon^2}\end{aligned}\tag{40b}$$

A comparison between the use of equations (39) and equations (40) will be made later.

Unit load. - Three approaches may be advanced for determining the downwash velocities that are produced by a unit load:

- 1.) Direct formal evaluation by equation (22), as in reference 1.
- 2.) An approach which is based on Scheme II, and which makes use of equation (28); the line source distribution of potential dipoles due to the unit load and given by this equation is replaced by "equivalent" concentrated dipoles. The velocities due to all these concentrated potential dipoles are then superimposed to give the downwash due to the unit load.
- 3.) An approach which makes use of equation (13) and equation (34). As in the determination of equations (35), (36), and (37), this approach greatly simplified the determination of the downwash values due to a unit load, and in the course obviates any problem with singularities. The remainder of this section is devoted mainly to the development of the basic notions of this approach.

By means of figure 7 we give a quick and overall insight to the basic concepts of the third approach. A detailed consideration will then follow. Consider a unit load: by the anti-symmetric property of p , we regard this load to be split equally between the upper and lower half planes, sketch (b). With respect to the associated pressure dipole representation, we take note of the explicit appearance, a "z" in equation (16) (and in equations (17) and (18)). The potential due to the unit load is given by equation (13). In the region $y \neq 0$, the potential is zero at $z = 0$, and hence, from equation (34), the vertical velocity is given by

$$w = \frac{\phi(z)}{z}\tag{41}$$

Thus, near the x-y plane and for $y \neq 0$, ϕ is a direct measure of w , see sketches (c), (d), and (e). The limiting form as $z \rightarrow 0$ follows easily. We let the z of equation (41) cancel the z in the dipole pressure equation, and let $z = 0$ elsewhere; the vertical velocities are, thus, effectively given

as the x-integration of equation (16) with the z removed. For $y = 0$ and behind the unit load ($x > 0$), a $\phi(0)$ exists, as given by equation (14). The value is easy to establish, being related to a simple Dirac-type integration through the upper load of $1/2$, sketch (g). Application of equation (34) yields w , sketch (h); effectively, the right-hand branch of $\phi(z)$ is sheared downward an amount $\phi^+(0)$. The magnitude of $\phi^+(0)$ is found through the evaluation of a rather simple indeterminate form at $x = \infty$. The limiting value of w as $z \rightarrow 0$ for this slice is also found easily, sketch (i). It is to be noted that ahead of the unit load there is no $\phi(0)$; the evaluation of w for this region is, therefore, as simple as for $y \neq 0$. Further, the value of $\phi(z)$ for positive x can be shown to be given in terms of $\phi(z)$ for negative x . Thus, the determination of w behind the unit load can be expressed simply in terms of the w ahead of the load and the constant $\phi^+(0)$. The development of the velocities by the concepts shown in figure 7 is considered significant; thus, we can virtually form a visual picture of how the velocities develop.

With this background, let us now consider a unit pressure dipole in detail. We treat first the regions $y \neq 0$. Substitute equation (16) into equation (13), apply equation (34), and let the remaining z 's = 0. Since $\phi(0) = 0$ in this region of concern, the result for w is immediate; thus,

$$w = K = \frac{\beta^2}{4\pi\rho_0 U} e^{-\frac{i\omega x}{U}} \int_{-\infty}^x \frac{1}{R^3} \left(1 + \frac{i\omega R}{a\beta^2}\right) e^{\frac{i-\omega}{a\beta^2} \left(\frac{\xi}{M} - R\right)} d\xi \quad (42)$$

where $R = \sqrt{x^2 + \beta^2 y^2}$. The notation K has been introduced because the expression is a form, here greatly simplified, of the kernel function. With equation (18) and $\omega = 0$, the result is simply

$$\begin{aligned} w &= \frac{1}{4\pi\rho_0 U} \int_{-\infty}^x \frac{d\xi}{(\xi^2 + y^2)^{3/2}} \\ &= \frac{1}{4\pi\rho_0 U} \frac{1}{y^2} \left(1 + \frac{x}{\sqrt{x^2 + y^2}}\right) \end{aligned} \quad (43)$$

For use in the grid system schemes advanced in this report, we desire average values over equally spaced y -intervals, in accordance with equation (25). We have, therefore, the following expressions defining the modified kernel function for regions

$y \neq 0$:

For a subsonic point load, $\omega \neq 0$,

$$\bar{K} = \bar{w}(x, y_0) =$$

$$= \frac{\beta^2}{4\pi\rho_0 U \lambda} e^{-\frac{i\omega x}{U}} \int_{y_0 - \frac{\lambda}{2}}^{y_0 + \frac{\lambda}{2}} \int_{-\infty}^x \frac{1}{R^3} \left(1 + \frac{i\omega R}{a\beta^2} \right) e^{\frac{i\omega}{a\beta^2} \left(\frac{\xi}{M} - R \right)} d\xi dy \quad (44)$$

and for a point load with $M = 0$, $\omega = 0$,

$$\bar{K} = \bar{w} =$$

$$= \frac{1}{4\pi\rho_0 U} \left[\frac{1}{y_0^2 - \frac{\lambda^2}{4}} + \frac{1}{\lambda x} \frac{\sqrt{(y_0 - \frac{\lambda}{2})^2 + x^2}}{y_0 - \frac{\lambda}{2}} - \frac{1}{\lambda x} \frac{\sqrt{(y_0 + \frac{\lambda}{2})^2 + x^2}}{y_0 + \frac{\lambda}{2}} \right] \quad (45)$$

For our grid system, we use $y_0 = n\lambda$, with $n = 1, 2, 3, \dots$. Numerical evaluation of equation (44) to give tabulated results for universal application, therefore, is needed.

For the region along and including $y = 0$, it is convenient to proceed in terms of a general notation. Let equation (13) be represented by

$$\phi(x, y, z) = \frac{1}{\rho_0 U} e^{-\frac{i\omega x}{U}} I(x, y, z) \quad (46)$$

where

$$I = - \int_{-\infty}^x e^{i\omega\xi/U} p(\xi, y, z) d\xi \quad (47)$$

An examination of the integral I in conjunction with the pressure dipole expressions given by equations (16) through (18) reveals that the integrand may be expressed in terms of even and odd functions of x as follows:

$$-e^{\frac{i\omega\xi}{U}} p(\xi, y, z) = f(\xi) + g(\xi)$$

where f is an even function and g is odd. The integral I thus may be written

$$I(x, y, z) = F(x, y, z) + G(x, y, z) \quad (48)$$

where

$$F(x, y, z) = \int_{-\infty}^x f(\xi) d\xi \quad (49a)$$

$$G(x, y, z) = \int_{-\infty}^x g(\xi) d\xi \quad (49b)$$

Because f is even and g is odd, the following properties exist:

$$\left. \begin{aligned} I(\infty) &= F(\infty) \\ F(x_1) &= F(\infty) - F(-x_1) \\ G(x_1) &= G(-x_1) \\ F(-\infty) &= G(-\infty) = G(\infty) = 0 \end{aligned} \right\} \quad (50)$$

in which the argument refers to the x values. With equation (34) in mind, we also establish the function $\phi(x, y, 0)$, the intensity of the dipole line source on the + side of the x - y plane aft of the unit load. This function, as obtained from equation (14), or as given by $-1/2$ the value indicated by equation (28) with $x_r = 0$, may be written

$$\phi(x, y, 0) = \frac{1}{\rho_0 U} e^{-\frac{i\omega x}{U}} \frac{1}{2} \delta_y(0) l(x - 0) \quad (51)$$

where $l(x - 0)$ denotes a unit step at the origin in the x -direction, and $\delta_y(0)$ denotes a Dirac function in the y -direction at $y = 0$. With equations (34), (46), (48), and (51), the vertical velocity may be written as

$$w = \frac{\phi(x, y, z) - \phi(x, y, 0)}{z} = \frac{1}{\rho_0 U} e^{-\frac{i\omega x}{U}} \frac{F + G - \frac{1}{2} \delta_y(0) l(x - 0)}{z} \quad (52)$$

We integrate this equation so as to give the average vertical velocities that exist in a band of width λ centered over the x -axis; thus

$$\bar{w}(x, z) = \frac{1}{\rho_0 U} e^{-\frac{i\omega x}{U}} \frac{1}{z} \left[\bar{F}(x, z) + \bar{G}(x, z) - \frac{1}{2\lambda} l(x - 0) \right] \quad (53)$$

where

$$\bar{F}(x, z) = \frac{1}{\lambda} \int_{-\lambda/2}^{\lambda/2} F(x, y, z) dy \quad (54a)$$

$$\bar{G}(x, z) = \frac{1}{\lambda} \int_{-\lambda/2}^{\lambda/2} G(x, y, z) dy \quad (54b)$$

We note that the $\delta_y(0)$ function has been absorbed. For negative x values, say $x = -x_1$, equation (53) becomes

$$\bar{w}(-x_1, z) = \frac{1}{\rho_0 U} e^{-\frac{i\omega x_1}{U}} \frac{1}{z} \left[\bar{F}(-x_1, z) + \bar{G}(-x_1, z) \right] \quad (55)$$

For positive x , say $x = x_1$, equations (50) and (54) can be used to rewrite equation (53) in the form

$$\bar{w}(x_1, z) = \frac{1}{\rho_0 U} e^{-\frac{i\omega x}{U}} \frac{1}{z} \left[\bar{I}(\infty) - \bar{F}(-x_1, z) + \bar{G}(-x_1, z) - \frac{1}{2\lambda} \right] \quad (56)$$

thus expressing w for plus x in terms of w for negative x .

We now consider the limiting value of these expressions as $z \rightarrow 0$. By the process indicated earlier in this section, the functions \bar{F}/z and \bar{G}/z reduce easily to the following

$$\begin{aligned} A(-x) &= \lim_{z \rightarrow 0} \frac{\bar{F}(-x, z)}{z} = \\ &= \frac{\beta^2}{4\pi\lambda} \int_{-\lambda/2}^{\lambda/2} \int_{-\infty}^{-x} \frac{1}{R^3} \left(1 + \frac{i\omega R}{a\beta^2}\right) e^{-\frac{i\omega R}{a\beta^2}} \cos \frac{\omega M \xi}{a\beta^2} dy d\xi \quad (57a) \end{aligned}$$

$$\begin{aligned} B(-x) &= \lim_{z \rightarrow 0} \frac{\bar{G}(-x, z)}{z} = \\ &= \frac{i\beta^2}{4\pi\lambda} \int_{-\lambda/2}^{\lambda/2} \int_{-\infty}^{-x} \frac{1}{R^3} \left(1 + \frac{i\omega R}{a\beta^2}\right) e^{-\frac{i\omega R}{a\beta^2}} \sin \frac{\omega M \xi}{a\beta^2} dy d\xi \quad (57b) \end{aligned}$$

It is noted that these equations are contained in equation (44) as demonstrated by the following steps: suppress the factor $\frac{1}{\rho_0 U} e^{-i\omega x/U}$, let $y_0 = 0$, and split the integral into a cosine and a sine part.

The remaining terms of equation (56) are combined to form the constant

$$C = \frac{1}{z} \left[\bar{I}(\infty) - \frac{1}{2\lambda} \right] \quad (58)$$

By equations (47) and (16), and with a y -integration, the definition of $\bar{I}(\infty)$ is

$$\bar{I}(\infty) = \frac{1}{\lambda} \int_{-\lambda/2}^{\lambda/2} \int_{-\infty}^{\infty} e^{\frac{i\omega \xi}{U}} \frac{\beta^2 z}{4\pi R^3} \left(1 + \frac{i\omega R}{a\beta^2}\right) e^{-i\omega \frac{-M\xi + R}{a\beta^2}} d\xi dy$$

where $R = \sqrt{x^2 + \beta^2(y^2 + z^2)}$. The ξ -integration can be made by means of transform 917.8 in reference (3), yielding the result

$$\bar{I}(\infty) = \frac{1}{\lambda} \int_{-\lambda/2}^{\lambda/2} \frac{z}{2\pi} \frac{1}{\sqrt{y^2 + z^2}} \frac{\omega}{U} K_1 \left(\frac{\omega}{U} \sqrt{y^2 + z^2} \right) dy \quad (59)$$

For small values of $\frac{\omega}{U} \sqrt{y^2 + z^2}$, as will be the case in practice, this expression reduces to

$$\bar{I}(\infty) = \frac{1}{\lambda} \int_{-\lambda/2}^{\lambda/2} \frac{z}{2\pi} \frac{1}{y^2 + z^2} dy$$

$$\bar{I}(\infty) = \frac{1}{\lambda\pi} \tan^{-1} \frac{\lambda}{2z} \quad (60)$$

With this equation, C becomes

$$C = \frac{1}{\pi z \lambda} \left(\tan^{-1} \frac{\lambda}{2z} - \frac{\pi}{2} \right) \quad (61a)$$

or in the limit as $z \rightarrow 0$

$$C = -\frac{2}{\pi \lambda^2} \quad (61b)$$

In summary, we find the following equations apply for the average velocity along the grid band that is centered over $y = 0$:

$$\bar{K} = \bar{w}(-x_1, 0) = \frac{1}{\rho_0 U} e^{-\frac{i\omega x_1}{U}} \left[A(-x_1) + B(-x_1) \right], \quad x = -x_1 \quad (62a)$$

$$\bar{K} = \bar{w}(x_1, 0) = \frac{1}{\rho_0 U} e^{-\frac{i\omega x_1}{U}} \left[-A(-x_1) + B(-x_1) - \frac{2}{\pi \lambda^2} \right], \quad x = x_1 \quad (62b)$$

These equations and equation (44) thus define the complete modified kernel function of the present report and are for use in equation (26) of Scheme I.

It is noted that equations analogous to equations (62) apply also for the case of 2-d flow; they are somewhat simpler

and differ in the following three specific ways: (1) the y-integration leading to equation (53) is, of course, not involved; (2) the factor $1/2$ would appear in place of the factor $1/2\lambda$ in equation (53); and (3) the constant C , as given by equation (61a) would be different. A later example will illustrate these points.

BLANK PAGE

SECTION V

EXAMPLE SPECIFIC CASES FOR K

Case 1: 2-dimensional incompressible steady flow ($\omega = 0$).-
To bring out some interesting and instructive facts, determination of the vertical velocity produced by a unit load will be illustrated by five different techniques mentioned in this paper.

Solution 1:

Use is made here of equations analogous to equations (57) and (62). For this case we find

$$A(x) = -\frac{1}{2\pi x}$$

$$B(x) = 0$$

$$C = 0$$

From equations (62), these lead to a single expression for w given by

$$w = \frac{-1}{2\pi\rho_0 Ux} \quad (63)$$

which agrees with the known exact solution to the problem.

Solution 2:

This solution is based on Scheme II, and is presented with the aid of figure 8. For the unit load the wake potential is given simply by (see equation (28))

$$\phi_0 = -\frac{1}{\rho_0 U} l(x - 0)$$

The strength of the equivalent concentrated potential dipoles spaced at equal intervals ϵ is thus

$$\phi = \frac{\epsilon}{\rho_0 U}$$

The w 's from each of these dipoles are given by equations (39); the values are tabulated on respective lines below the dipoles.

The superimposed total w is shown near the bottom of figure 8; it is noted that the results are the same as given by equation (63), thus showing that this method also leads to the exact answer.

Solution 3:

This solution proceeds as in the second solution, but makes use of equations (40) instead of equations (39). The results obtained by this method are shown in figure 9, curve (b), along with the exact results just derived, curve (a). We see from this comparison the effect of not using average values of velocities over each interval in the representation of w for each concentrated dipole.

Solution 4:

In this solution we determine w by equation (34), and keep z finite to show the influence of not passing to the limit $z \rightarrow 0$. Equations analogous to equations (55) and (56) are involved. With equations (13), (14) and (17) the result can be shown to be

$$\begin{aligned}\phi(x, z) &= \frac{1}{2\pi\rho_0 U} \int_{-\infty}^x \frac{z d\xi}{\xi^2 + z^2} \\ &= \frac{1}{2\pi\rho_0 U} \left(\tan^{-1} \frac{x}{z} + \frac{\pi}{2} \right)\end{aligned}$$

$$\phi(x, 0) = \frac{1}{2\rho_0 U} l(x - 0)$$

$$\begin{aligned}w &= \frac{\phi(x, z) - \phi(x, 0)}{z} = \frac{1}{2\pi\rho_0 U} \frac{1}{z} \left[\tan^{-1} \frac{x}{z} + \frac{\pi}{2} - \pi l(x - 0) \right] \\ &= -\frac{x}{z} \left[\tan^{-1} \frac{x}{z} + \frac{\pi}{2} - \pi l(x - 0) \right] w_e \quad (64)\end{aligned}$$

where w_e is the exact result given by equation (63). The results are shown in figure 10 for positive x only, since the results for negative x would be the same. We note the interesting fact that as long as $\frac{x}{z} > 3$, the approximate solution (z finite) is essentially the same as the exact solution.

Solution 5:

In this solution we show the effect of wake termination. The wake strength is given by

$$\phi_o(x) = -\frac{1}{\rho_o U} l(x - o)$$

With equation (17) we find the field potential for a finite length wake to be

$$\phi(x, z) = \frac{1}{2\pi\rho_o U} \int_0^b \frac{z d\xi}{(x - \xi)^2 + z^2}$$

where b represents the point downstream of wake cutoff. This equation yields

$$\phi(x, z) = \frac{1}{2\pi\rho_o U} \left(\tan^{-1} \frac{x}{z} - \tan^{-1} \frac{x - b}{z} \right)$$

The vertical velocity as determined from this equation is

$$w = \lim_{z \rightarrow 0} \frac{\partial \phi}{\partial z} = -\frac{1}{2\pi\rho_o U x} \left(1 + \frac{x}{b - x} \right) \quad (65)$$

This equation shows that w will be essentially the exact value if $\frac{x}{b-x}$ is kept small. A useful guide is afforded by this equation; thus, the term $\frac{x}{b-x}$ shows that if x is kept to within .05 b , for example, then errors in w due to wake termination will be less than 5 percent. This observation, of course, applies to the 2-dimensional steady flow problem. For the oscillatory case, the errors in w due to wake termination should be even less.

Case 2: 2-dimensional incompressible flow, $\omega \neq 0$. For this case equations corresponding to equations (57) are

$$A(-x) = \frac{1}{2\pi} \int_{-\infty}^{-x} \frac{\cos \frac{\omega \xi}{U}}{\xi^2} d\xi = \frac{\cos \frac{\omega x}{U}}{2\pi x} - \frac{\omega}{2\pi U} \left[\frac{\pi}{2} - \text{Si} \left(\frac{\omega x}{U} \right) \right] \quad (66a)$$

$$B(-x) = \frac{i}{2\pi} \int_{-\infty}^{-x} \frac{\sin \frac{\omega \xi}{U}}{\xi^2} d\xi = -i \frac{\sin \frac{\omega x}{U}}{2\pi x} + i \frac{\omega}{2\pi U} \text{Ci}\left(\frac{\omega x}{U}\right) \quad (66b)$$

Because 2-dimensional flow is involved, the constant C for this case is different than that given by equations (58) and (61). Here, in place of the \bar{I} in equation (56), we have

$$I(\infty) = \frac{1}{2\pi} \int_{-\infty}^{\infty} \frac{ze^{\frac{i\omega \xi}{U}}}{\xi^2 + z^2} d\xi = \frac{1}{2} e^{-z|\frac{\omega}{U}|}$$

and in place of the factor $\frac{1}{2\lambda}$ we have simply $1/2$; the constant C is thus given by

$$\begin{aligned} C &= \lim_{z \rightarrow 0} \frac{1}{2} \frac{e^{-z|\frac{\omega}{U}|} - 1}{z} \\ &= -\frac{1}{2} \frac{\omega}{U} \end{aligned}$$

Using equations (66) and this value of C in place of the $-\frac{2}{\pi\lambda^2}$ term in equations (62), we find

$$w(x) = \frac{1}{2\pi p_0 U} \frac{1}{x} \left\{ -1 + \frac{i\omega x}{U} e^{-\frac{i\omega x}{U}} \left[\text{Ci}\left(\frac{\omega x}{U}\right) + \frac{i\pi}{2} + i \text{Si}\left(\frac{\omega x}{U}\right) \right] \right\} \quad (67)$$

which agrees with the known solution of this problem as determined by other exact means; it is interesting to note that this equation applies for both negative and positive x .

Case 3: 3-dimensional incompressible flow, $\omega = 0$. - The solution desired in this case is for the average w over equally spaced y -intervals, as would be used in equation (26). The equation for w for this case applying in the region $y \neq 0$ has already been derived, equation (45). For $y = 0$, we find

$$A(-x) = \frac{1}{\pi\lambda^2} \left(-1 + \sqrt{\frac{x^2 + \frac{\lambda^2}{4}}{x}} \right)$$

$$B(-x) = 0$$

$$C = -\frac{2}{\pi\lambda^2}$$

Equations (62) therefore yields

$$\bar{w}(x, 0) = \frac{-1}{\pi\rho_0 U\lambda^2} \left(1 + \sqrt{\frac{x^2 + \frac{\lambda^2}{4}}{x}} \right) \quad (68)$$

an equation that holds for both positive and negative x . It should be noticed that for negative x , this equation yields the same value of \bar{w} as does equation (45), as it should. A rather significant observation may be made at this point. It is noted that equations (63), (67) and (68) apply over the complete range of x , due to the fact that x appears in an explicit way outside of certain terms. Thus, in a remarkable way, the solution for w for negative x , for which no consideration of a singularity has to be given, appears also to apply for positive x if exact integration can be made. In such cases, then, solution appears to be possible without having to give any consideration whatsoever to singularities.

Case 4: 2-dimensional incompressible flow, $\omega = 0$, as derived from discrete equal loads.- In this case we make use of the results of Case 3 to derive results for 2-dimensional flow by considering an infinite array of concentrated loads equally spaced in the y -direction, rather than using a uniform line source, see figure 11. To give the results in terms of an effective loading of unity per unit length in the y -direction we let each of the concentrated loads have a magnitude λ . The superposed \bar{w} due to all the loads follows from equations (45) and (68) as

$$\bar{w} = \frac{-\lambda}{\pi\rho_0 U\lambda^2} \left(1 + \sqrt{\frac{x^2 + \frac{\lambda^2}{4}}{x}} \right) + 2 \frac{\lambda}{4\pi\rho_0 U} \frac{1}{\lambda^2} \sum_{n=1}^{\infty} \left[\frac{4}{4n^2 - 1} + \frac{\lambda}{x} \sqrt{\frac{(2n-1)^2 + 4 \frac{x^2}{\lambda^2}}{2n-1}} - \frac{\lambda}{x} \sqrt{\frac{(2n+1)^2 + 4 \frac{x^2}{\lambda^2}}{2n+1}} \right] \quad (69)$$

This equation may be investigated quite readily for x very small and x very large; the known infinite summation

$$\frac{1}{2} = \sum_{n=1}^{\infty} \frac{1}{4n^2 - 1}$$

provides an aid. The results are found to be simply

$$\bar{w} = \frac{-1}{2\pi\rho_0 Ux}, \quad x \text{ small}$$

$$\bar{w} = 0, \quad x = \infty$$

These results indicate a rather remarkable fact; thus, in spite of the fact that we have represented the uniform line source by an infinite array of concentrated loads, we find the solution to be the exact solution for small and large x . The use of average values of w over each interval evidently retains all the essential intelligence of the flow-field. Equation (69) has not been investigated here for intermediate x values, but it is expected to yield exact results in this range also.

SECTION VI

EXAMPLE TREATMENT OF WINGS

Illustrations of the application of the numerical grid schemes of this paper are shown in this section; for brevity, and because exact solutions are known, the examples are given in terms of a 2-dimensional airfoil in steady flow.

Example 1:

In this example we use only a single concentrated load. The grid spacing ϵ becomes the chord, c . We place the load at the quarter-chord point and consider w at $3/4c$ as shown in figure 12(a) (our insight on these locations is based on prior knowledge of airfoil behavior characteristics). By equation (63) we find that

$$w = \frac{-L}{\pi \rho_0 U c}$$

leading to the inverted form

$$L = -\pi \rho_0 U c w$$

For a constant angle of attack α , we have $w = -U\alpha$, and thus

$$L = \pi \rho_0 U^2 c \alpha$$

This is the known exact solution to the problem. The pitching moment will also be correct because the load was placed at the quarter-chord. Thus we see the rather remarkable fact that the correct lift and moment were obtained using only a single load and a single downwash point. We have treated this seemingly absurd case because it provides a key guide on how to handle the next examples.

Example 2:

In this example we use 2 loads and 2 downwash points as shown in figure 12(b). With example 1 as a guide, we have located these loads and w points in the particular locations shown; note the locations with care. From equation (63) the appropriate equations for this case are found to be

$$\begin{vmatrix} w_1 \\ w_2 \end{vmatrix} = \frac{2}{\pi \rho_0 U c} \begin{vmatrix} -1 & 1 \\ -\frac{1}{3} & -1 \end{vmatrix} \begin{vmatrix} L_1 \\ L_2 \end{vmatrix}$$

Inverted, these equations appear

$$\begin{vmatrix} L_1 \\ \\ L_2 \end{vmatrix} = \frac{\pi \rho_0 U c}{8} \begin{vmatrix} -3 & -3 \\ 1 & -3 \end{vmatrix} \begin{vmatrix} w_1 \\ \\ w_2 \end{vmatrix}$$

For a constant angle of attack, for which $w_1 = w_2 = -U\alpha$, we find

$$L_1 = \frac{3}{4} \pi \rho_0 U^2 c \alpha$$

$$L_2 = \frac{1}{4} \pi \rho_0 U^2 c \alpha$$

These values yield a total lift and a moment arm referred to the leading edge as follows

$$L = \pi \rho_0 U^2 c \alpha$$

$$e = \frac{\frac{3}{4} \frac{c}{8} + \frac{1}{4} \frac{5c}{8}}{\frac{3}{4} + \frac{1}{4}} = \frac{c}{4}$$

These values also correspond to the exact solution.

Example 3:

This example considers 3 loads and 3 downwash points, located as shown in figure 12(c). The guideline being evolved, and which appears to be remarkably successful, is as follows: divide the chord into as many equal intervals as there are loads; locate a load at each 1/4 point of an interval, a downwash point at each 3/4 point. The equations that result for this case are:

$$\begin{vmatrix} w_1 \\ w_2 \\ w_3 \end{vmatrix} = \frac{3}{\pi \rho_0 U c} \begin{vmatrix} -1 & 1 & \frac{1}{3} \\ -\frac{1}{3} & -1 & 1 \\ -\frac{1}{5} & -\frac{1}{3} & -1 \end{vmatrix} \begin{vmatrix} L_1 \\ L_2 \\ L_3 \end{vmatrix}$$

$$\begin{array}{c|c} \begin{array}{c} L_1 \\ L_2 \\ L_3 \end{array} & = \frac{\pi \rho_0 U c}{64} \begin{array}{ccc} -15 & -10 & -15 \\ 6 & -12 & -10 \\ 1 & 6 & -15 \end{array} \begin{array}{c} w_1 \\ w_2 \\ w_3 \end{array} \end{array}$$

For a constant angle of attack, with $w_1 = w_2 = w_3 = -U\alpha$, we find

$$L_1 = \frac{5}{8} \pi \rho_0 U^2 c \alpha$$

$$L_2 = \frac{2}{8} \pi \rho_0 U^2 c \alpha$$

$$L_3 = \frac{1}{8} \pi \rho_0 U^2 c \alpha$$

which yield a total lift and a moment arm relative to the leading edge of

$$L = \pi \rho_0 U^2 c \alpha$$

$$\epsilon = \frac{c}{4}$$

Again the exact results are obtained. By induction, we may expect an exact solution for all smaller intervals, if the loads and downwash points are located by the guideline stated at the beginning of this example. From these three examples we wish also to make the following observation thought significant. In all the three cases, downwash points have been chosen midway between the concentrated loads and in an aft direction, with surprisingly successful end results. No consideration has had to be made about flow or loading in the leading edge region. Essentially, we are saying that with this technique, we care not a wit about the mathematical character of the loading at the leading edge, nor whether w is satisfied in this region. Apparently flow is controlled predominantly by the aft regions of the airfoil. Perhaps this is a reflection of the Kutta condition at the trailing edge, which governs the strength of the entire flow.

Example 4:

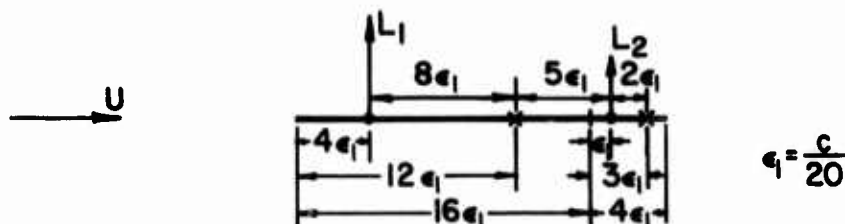
For this example, Scheme II was applied to the airfoil case treated in Example 3. A detailed listing of the solution is

not considered necessary, but solution proceeds in the manner depicted by figures 5 and 8. Again considering the constant angle of attack case, it was found that exact results for lift and moment were also obtained by this approach. A main point of the example is the reminder that, since the complete potential system is constructed by this approach, it is possible to establish all components of flow velocity anywhere in the field, such as in the vicinity of a tail.

SECTION VII

REMARKS ON GRID LAYOUT

The concepts advanced in this paper have not been exercised sufficiently to permit definite guidelines to be stated on wing grid layout. Some suggestions on how to lay out the grid system can be made, however. It is felt that a matrix somewhere between a 4 x 4 matrix (four chordwise intervals by four semispan intervals) and a 10 x 10 matrix should adequately handle most lifting surfaces. The thought that the matrix should be square is not to be inferred from these numbers. Suggested layouts are shown in figure 13. For untapered straight or swept wings and for deltas with a straight trailing edge, a simple rectangular grid pattern can be used, figure 13(a) and 13(b). For deltas with a swept forward trailing edge, an array consisting of rectangular blocks of one size in the leading edge region and rectangular blocks of another size in the trailing edge region might be employed, figure 13(b); these smaller trailing edge blocks represent the type that might also be used in the treatment of control surfaces. An interesting question arises at this point. Can intervals of different lengths be mixed? As a means for shedding some light on this question, the wing system shown in the following sketch was analyzed.



The airfoil was arbitrarily divided into two intervals - the front interval being $\frac{4}{5} c$ long, the aft $\frac{1}{5} c$ long. A load and a downwash point were located in each interval according to the rule of thumb used in the example airfoil cases; specifically, the load is placed at the $\frac{1}{4}$ point of the interval, the downwash at the $\frac{3}{4}$ point. The system was analyzed, as in the example cases, with the following results:

$$L_1 = .923 \pi \rho_0 U^2 c \alpha$$

$$L_2 = .077 \pi \rho_0 U^2 c \alpha$$

$$L = \pi \rho_0 U^2 c \alpha$$

$$e = c/4$$

Amazingly, the exact answer is found again. (There appears to be some magic associated with the $1/4$ and $3/4$ points.) Evidently, then, mixed interval size can be used to good advantage.

Figure 13(c) shows thoughts on tapered wings. We note that the blocks are of varying aspect ratios in this constant y-interval treatment. A variation of this scheme is shown in figure 13(d) wherein the y-interval is also varied to yield blocks of constant aspect ratio. The possible disadvantage of the layouts of figures 13(c) and 13(d) is that unequal intervals and a sheared grid system are involved, thereby increasing the task of evaluating the kernel function; this point, of course, does not become of too great a concern if the kernel function values are tabulated at frequent x and y intervals. In spite of the fact that the load and downwash points are not located in a rectangular array fashion, the layout scheme of figure 13(d) may turn out to be the preferred scheme. Of all the schemes, it is the least arbitrary, and it applies to all wings regardless of planform. The scheme also tends to distribute and group the loads more towards the tip sections, which probably are the most important in controlling aeroelastic behavior.

Figure 13(e) shows a possible gridwork for a trapezoidal-type wing; here, a fairly fine rectangular gridwork is used. Two additional points may be brought out in discussing this arrangement. One pertains to gridwork size in the inboard region. If small blocks are used throughout, then many chordwise blocks are found in this region. It, thus, may be worthwhile to increase the size of these inboard blocks as a means for decreasing the total number. In the example shown, 58 blocks would be involved if the same small size were used throughout. By only doubling the length of the inboard blocks, the number has been reduced to 38. This idea should especially apply if the wing is a cantilever, since the inboard region probably has little influence on determining the flow, and therefore should not require as detailed a treatment as for the tip region. A second point is that with the use of small blocks it probably isn't necessary to average the velocity in the y-direction for blocks remote to a load (as in equation (44)). The use of the w at the center of such blocks is probably accurate enough, thus lessening the chore of determining the kernel function. The effect of averaging or not averaging can be illustrated by equation (39a); the -1 in the denominator is a result of the averaging process, and without the -1 the equation would yield the velocity at the center of the interval. It can be seen that for n as small as 4, referring to a point just 4 intervals away, the neglect of the -1 changes the w -value by not even 2 percent.

How large should the intervals ϵ and λ be? The steady state example cases indicate that the interval may be quite large (even equal to the chord in one case). For oscillatory flow, however, definite wavelength patterns exist in the flow field, and these can be expected to have a bearing on interval size. We consider these wavelengths in the following as a means for establishing an upper limit to interval size. An examination of equation (16) indicates that three frequency components in the x-direction must be considered if evaluation is made by numerical techniques; namely,

$$\Omega_1 = \frac{\omega}{U}$$

$$\begin{aligned} \Omega_2 &= \frac{\omega(1 - M)}{\alpha\beta^2} \\ &= \frac{\omega M}{U(1 + M)} \quad , \quad \text{for } x \text{ positive, } R = x \end{aligned}$$

$$\begin{aligned} \Omega_3 &= \frac{\omega(1 + M)}{\alpha\beta^2} \\ &= \frac{\omega M}{U(1 - M)} \quad , \quad \text{for } x \text{ negative, } R = |x| \end{aligned}$$

The smallest wavelengths are associated with Ω_1 and Ω_3 and are given by

$$\lambda_1 = \frac{2\pi}{\Omega_1} = \frac{2\pi U}{\omega}$$

$$\lambda_3 = \frac{2\pi}{\Omega_3} = \frac{2\pi U(1 - M)}{\omega M}$$

To maintain a reasonably accurate numerical procedure, we reason that the interval ϵ should be something in the order of $1/12$ or less of the shortest wavelength; (effectively, we are saying that 12 equally spaced values or more should define one cycle of a sine wave reasonably well). Thus

$$\epsilon \leq \frac{2\pi U}{12\omega}$$

or

$$c \leq \frac{2\pi U(1 - M)}{12\omega M}$$

whichever is the shorter. Written in terms of the chord and reduced frequency, we have

$$\frac{\epsilon}{c} \leq \frac{\pi}{12k}$$

$$\frac{\epsilon}{c} \leq \frac{\pi}{12k} \frac{1-M}{M}$$

The first of these equations governs for $0 < M \leq 1/2$; the second for $M \geq 1/2$; values of ϵ/c as obtained from these expressions are given in the following tabulation.

<u>k</u>	<u>M = 0 - .5</u>	<u>.6</u>	<u>.8</u>
.05	$\epsilon/c = 5.83$	3.48	1.31
.1	2.62	1.74	.654
.2	1.31	.882	.327
.3	.882	.582	.196
.4	.654	.436	.164
.5	.523	.348	.131

A similar treatment for the y-direction indicates only a single frequency and the following results:

$$\Omega_y = \frac{\omega M}{U \beta}$$

$$\frac{\lambda}{c} = \frac{\pi}{12k} \frac{\sqrt{1-M^2}}{M}$$

<u>k</u>	<u>M = .1</u>	<u>.2</u>	<u>.4</u>	<u>.6</u>	<u>.8</u>
.05	$\lambda/c = 52.1$	25.6	12.0	7.0	3.93
.1	26.1	12.8	6.0	3.5	1.96
.2	13.0	6.4	3.0	1.74	.98
.3	8.8	4.32	2.02	1.18	.66
.4	6.52	3.2	1.50	.87	.49
.5	5.22	2.56	1.20	.70	.39

These results indicate that the wavelength components of the flow are not of prime concern in establishing interval size, except in the range of high k and high subsonic Mach number values. For the lower k and M values, other considerations, such as the geometry of motion of the airfoil, would govern. With respect to a plunging, pitching, and possibly deforming airfoil, for example, the following question is of concern. How many downward points should be used to represent the motion? From a curve-fitting point of view, it is reasoned that a minimum of 4 to 5 points should be used to give adequate representation of motion across the chord. Thus a minimum of 4 chordwise intervals is suggested; by similar consideration, at least 4 spanwise stations should be used. Taking into account these various thoughts on interval size, and until more experience on the practical application of the grid scheme is available, we might state the following rule of thumb: for low k and low M values, use 5 or 6 chordwise and 5 or 6 spanwise intervals, and for the high k and M ranges, use intervals as indicated by the ϵ/c and λ/c tabulations given earlier in this section.

BLANK PAGE

SECTION VIII

FREQUENCY RESPONSE AND FLUTTER DETERMINATION

One of the features of the schemes of this paper is that the equation relating P to w is ideally suited for both of the basic types of aeroelastic formulations that are normally employed, specifically, for either the approach which is in terms of discrete masses and influence coefficients or the approach which uses modal functions and a Lagrangian treatment. By way of example, we show in the following how the frequency response functions of an airplane due to sinusoidal gust encounter may be derived; the equations for flutter are in turn automatically derived.

In reading this section the reader should be aware that, to simplify the writing, considerable liberty has been taken with the matrix notation; it is abbreviated or inconsistent in places, and matrix elements are presented in a general sense only.

By discrete masses and influence coefficients.- Let the dynamical equations for sinusoidal motion of the complete airplane system be represented by the matrix equation.

$$[D]|Z_s| = \omega^2|m||Z_s| + |P_s| \quad (70)$$

where Z_s is the column matrix denoting the deflection at each of the discrete mass points (which may include the fuselage and tail as well as the wing), D is the operator which leads to total loading, m a diagonal mass matrix, and P_s the applied loading matrix. In the form presented, the equation applies either to a free-free system or to a restrained system such as a cantilever. For a sinusoidal gust, equation (24b) may be written

$$w = U \frac{\partial Z}{\partial x} + i\omega Z - e^{-i\frac{\omega x}{U}} \quad (71)$$

where x is the location of the downwash point relative to some convenient reference point such as the leading edge of the root chord of the wing. In general, the load and deflection points used for the dynamical treatment of the system may not be the same as those used for establishing the aerodynamic loads. By suitable interpolation formulae, however, these two load and deflection systems may be easily related, and we suppose that the transformations from one system to the other are given by

$$|P| = [T_1] |P_s| \quad (72a)$$

$$|Z_s| = [T_2] |Z| \quad (72b)$$

where T_1 and T_2 are in general rectangular matrices. Combining equations (26), (70), (71) and (72), we find

$$\bar{K} T_1 (D - \omega^2 m) T_2 Z = \left(U \frac{\partial}{\partial x} + i\omega \right) Z - e^{-i \frac{\omega x}{U}} \quad (73)$$

where, for simplicity in writing, the matrix notation has been dropped. Equation (73) in turn may be written

$$\left[\bar{K} T_1 (D - \omega^2 m) T_2 - \left(U \frac{\partial}{\partial x} + i\omega \right) \right] Z = - e^{-i \frac{\omega x}{U}}$$

or

$$D_1 Z = - e^{-i \frac{\omega x}{U}} \quad (74)$$

Inverted, we find the desired result for the frequency response function Z , thus

$$Z = - D_1^{-1} e^{-i \frac{\omega x}{U}} \quad (75)$$

From Z we may determine the frequency response function for other quantities of interest, such as acceleration or load at given points.

It is to be noted that this development was made in a way so as to make the inversion of the \bar{K} matrix unnecessary, see equation (74); thus the developments in this report appear all the more attractive. The D_1 matrix of equation (74) is obtained by matrix multiplication and addition of various matrices, each one of which is established in a straightforward way. Solution for the frequency response is thus reduced to a single inversion of the end result matrix D_1 , as shown by equation (75).

The equation describing flutter of the system follows directly from equation (74), being simply this equation with the right hand side set equal to zero.

By a modal function approach.- We assume that the response due to a sinusoidal gust input is expressed in terms of the natural modes Z_n of the airplane system according to the equation

$$Z = a_1 Z_1 + a_2 Z_2 + a_3 Z_3 + \dots \quad (76)$$

where the a_n 's are generalized coordinates. It is well established that a Lagrangian formulation in terms of equation (76) leads to the following basic response equation for a_n

$$M_n \ddot{a}_n + \omega_n^2 M_n a_n = \int p Z_n dS \quad (77)$$

where M_n is the generalized mass and ω_n is the natural frequency of the nth mode, and where p is the applied loading over the surface S . If equation (77) is applied to each of the modes considered, and if the loading p is expressed in terms of equivalent concentrated loads at various grid points, then, for the sinusoidal case of a_n , we can write the following matrix equation

$$\left[(\omega_n^2 - \omega^2) M_n \right] |a_n| = |Z_n| |P| \quad (78)$$

where $\left[(\omega_n^2 - \omega^2) M_n \right]$ is a simple diagonal matrix, a_n a column matrix, Z_n is a rectangular matrix built up from row matrices which express the deflection at each grid point for each mode Z_n , and P is a column matrix of the applied concentrated loads at each grid point. The simple matrix form of the generalized forces on the right hand side of equation (78) follows from equation (77) because of the Dirac function nature of each concentrated load. We now show two ways for proceeding with the solution. One method involves the inversion of the \bar{K} matrix and leads to a solution in terms of the a_n values. The other represents a very interesting different version, which avoids having to invert the \bar{K} matrix and which leads to a solution directly in terms of the P values. For both versions we make use of the matrix representation of equation (76) to express the deflection at each of the chosen grid points, namely

$$|z| = [z'_n] |a_n| \quad (79)$$

where $[z'_n]$ is a rectangular matrix in which each column represents the deflection at the various grid points in a given mode.

In the first version we combine equations (27) and (71), and (79) to obtain the loading as

$$|P| = [\bar{K}]^{-1} \left[U \frac{\partial}{\partial x} + i\omega \right] [z'_n] |a_n| - [\bar{K}]^{-1} |e^{-i \frac{\omega x}{U}}| \quad (80)$$

The substitution of this equation into equation (78) leads to the result

$$\begin{aligned} & \left[\left[(\omega_n^2 - \omega^2) M_n \right] - [z_n] [\bar{K}]^{-1} \left[U \frac{\partial}{\partial x} + i\omega \right] [z'_n] \right] |a_n| \\ & = - [z_n] [\bar{K}]^{-1} |e^{-i \frac{\omega x}{U}}| \end{aligned}$$

or

$$[E] |a_n| = - [z_n] [\bar{K}]^{-1} |e^{-i \frac{\omega x}{U}}| \quad (81)$$

Solution for a_n yields the frequency response functions for a_n . With the a_n 's established, various other frequency response functions, such as acceleration or load at a given point, follow readily.

In the second version we proceed by solving equation (78) for $|a_n|$, or

$$|a_n| = \left[\frac{1}{(\omega_n^2 - \omega^2) M_n} \right] [z_n] |P|$$

where solution follows simply because the square matrix on the left hand side of equation (78) is diagonal. The combination of this equation and equation (79) yields

$$|Z| = [Z'_n] \left[\frac{1}{(\omega_n^2 - \omega^2) M_n} \right] |Z_n| |P|$$

With this equation and equation (71), we find

$$|w| = \left[U \frac{\partial}{\partial x} + i\omega \right] [Z'_n] \left[\frac{1}{(\omega_n^2 - \omega^2) M_n} \right] |Z_n| |P| - \left| e^{-i \frac{\omega x}{U}} \right| \quad (82)$$

We now combine this equation with equation (26) by eliminating w , and find the following equation in terms of the P values only

$$\left[[\bar{K}] - \left[U \frac{\partial}{\partial x} + i\omega \right] [Z'_n] \left[\frac{1}{(\omega_n^2 - \omega^2) M_n} \right] |Z_n| \right] |P| = - \left| e^{-i \frac{\omega x}{U}} \right| \quad (83)$$

or

$$[H] |P| = - \left| e^{-i \frac{\omega x}{U}} \right|$$

Inverted, we find the frequency response values for P directly as

$$|P| = - [H]^{-1} \left| e^{-i \frac{\omega x}{U}} \right| \quad (84)$$

It is to be noted that the matrices leading to H are all very easy to establish, and thus this version appears especially attractive.

For flutter considerations by this modal approach we consider the homogeneous part of either equation (81) or (83); that is, we consider these equations with the right hand sides set equal to zero.

SECTION IX

CONCLUDING REMARKS

Most of the sections in this paper contain some discussion of the possible merits or advantages of the concepts developed. We therefore conclude with only a few additional remarks.

In this paper, we have advanced the concept of using concentrated loads to represent the aerodynamic loading on a lifting surface. Many variations of this idea may be conceived. For example, the distributed loading may be expressed in terms of various approximations, such as straight line or parabolic segments, with unknown values at various grid points. Equivalent concentrated loads can, in turn, be deduced from this representation. These concentrated loads can then be handled by the procedures developed in the paper, with the result that the downwash values are thus given in terms of the distributed load values. Whether this "apparent" refinement would represent an improvement or not, however, is not known. Another idea that may be of good practical use in application is the following. Consider a slice cut out of the wing in the x -direction and of width λ in the y -direction. Assume a pressure distribution on this slice that is uniform in the y -direction and represented by various pressure mode functions in the x -direction. For each of the pressure mode assumptions, establish the downwash for a number of points along the center line of the slice and along lines in the x -direction which are spaced at equal y -intervals λ ; these downwash values are then used for universal application thereafter. The application to any wing, for example, would be to consider a series of such slices placed side by side in such a way as to cover the planform; essentially, by this representation, we envision that the pressure distribution over the wing is given by smooth functions in the x -direction and by a succession of steps in the y -direction. Solution by this approach becomes simply a matter of determining by an equation analogous to equation (27) the magnitude of the x -pressure modes at each y station so as to yield the prescribed or desired downwash distribution.

With respect to limits on matrix size in the practical application of the schemes of this paper, we may find that there is no great concern over how large the matrices may be because of the capability of modern computing machines. Matrices as large as 10×10 or 10×20 may present no difficulty, for example; this point has a bearing on whether average values of w within an interval are used or not. Thus, if large matrices can be handled without difficulty, it may be as good or better to use a large matrix and no averaging of w as contrasted to the use of small matrices and average w values. A point of uncertainty on

matrix size should be mentioned, however. Because experience with the schemes has not yet been obtained on a broad basis, we don't know whether difficulties with numerics will be encountered. We don't know, for example, whether the large matrices may be ill-conditioned, thereby making inversion difficult. The evidence provided by the example cases of this paper indicates the matrices are not ill-conditioned, but whether this is also so for very large matrices has to be established. In spite of these questions on inversion, it is to be noted that the developments given in the preceding section show that aeroelastic problems may be solved without inversion of the K matrix; thus, the question of matrix inversion may, in reality, not be of concern.

We conclude by identifying in summary the pertinent equations for w which require numerical integration. These are equations (38), giving w for a subsonic dipole, and equations (44), (57), and (62) which represent the kernel function. These equations, expressed in a convenient, nondimensional form, should be evaluated for various $K = \omega c/2U$ and M values. A tabulation of results would provide a universal set of numbers and would obviate the necessity of evaluating the expressions in each new problem treated. Application of the techniques advanced in this paper to solve various oscillating flow problems would be a rather simple routine task.

REFERENCES

1. Watkins, Charles E., Runyan, Harry L., and Woolston, Donald E. "On the Kernel Functions of the Integral Equation Relating the Lift and Downwash Distributions of Oscillating Finite Wings in Subsonic Flow." NACA Report 1234, 1955. (Supersedes NACA TN 3131)
2. Garrick, I.E. "Nonsteady Wing Characteristics." Section F of Volume VII, Aerodynamics of Aircraft Components at High Speeds, Aeronautics Publication Program, Princeton University Press, Princeton, N.J., 1957.
3. Campbell, George A. and Foster, Ronald M. Fourier Integrals for Practical Applications. D. Van Nostrand Co., Inc., New York, 1954.

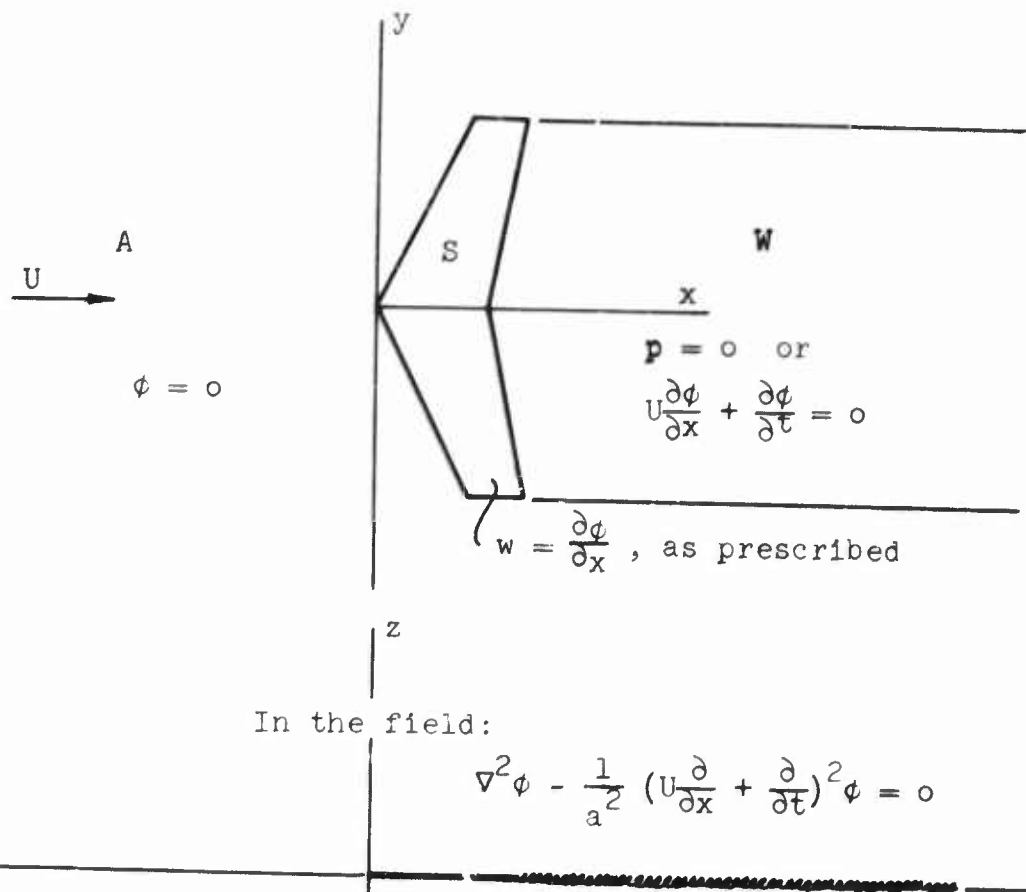


Figure 1. Regions of Concern and Boundary Conditions

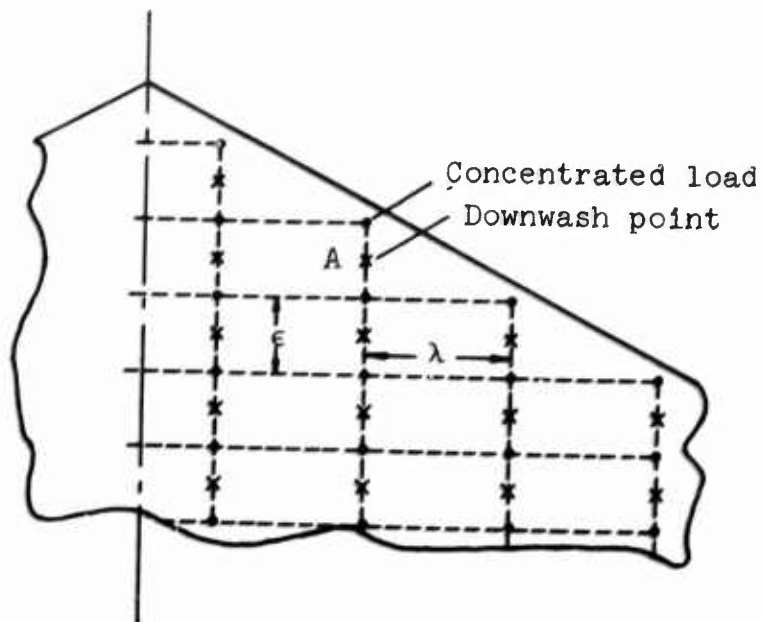
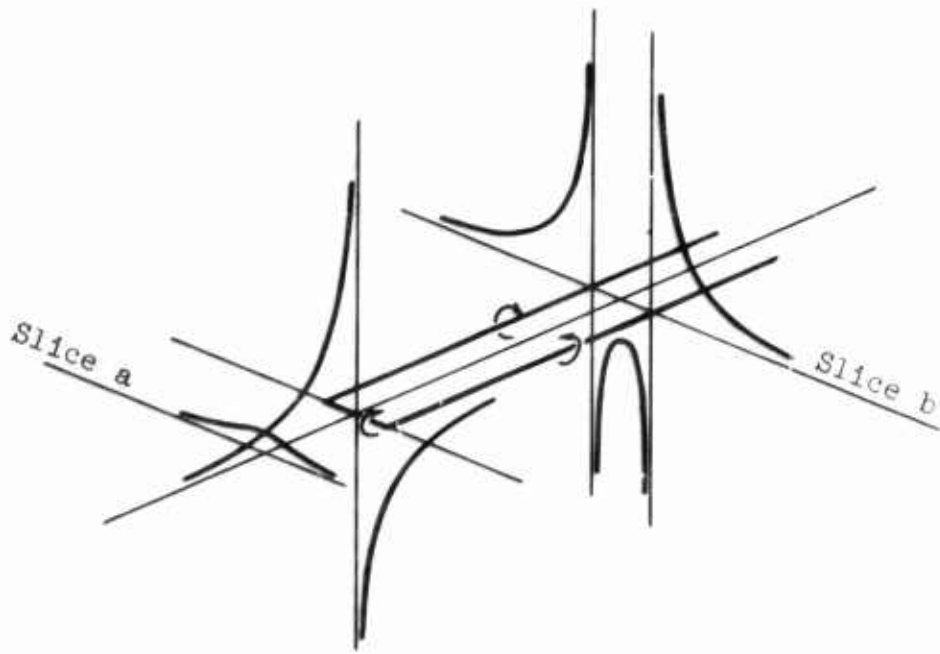
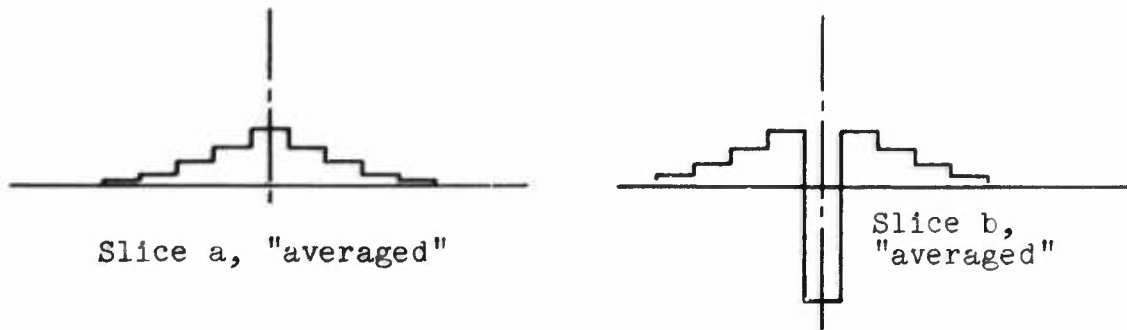


Figure 2. Grid Pattern Locating Concentrated Loads and Downwash Points

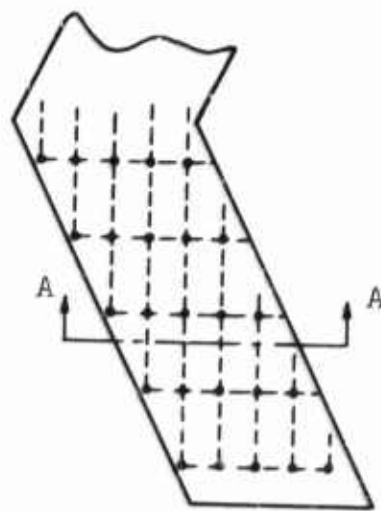


(a) Horseshoe vortex



(b) Averaged velocities

Figure 3. Vertical Velocity Field for a Narrow Horseshoe Vortex

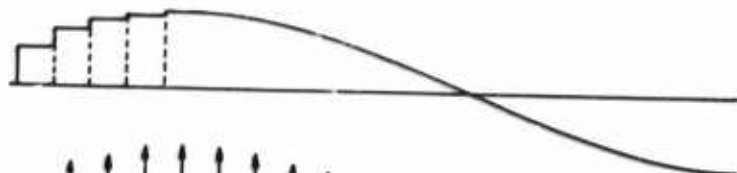


View A-A:

Concentrated loads:



ϕ_0 distribution

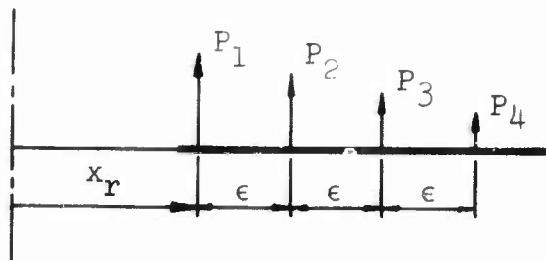


Equivalent

discrete ϕ_0 's



Figure 4. Basic Notions of Scheme II



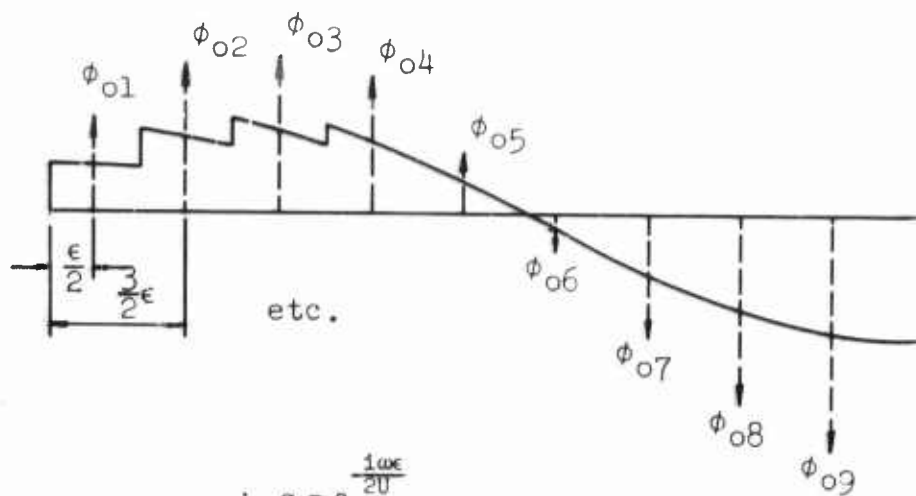
$$-\phi_1 = \frac{P_1}{\rho_0 U} e^{\frac{1\omega}{U}(x_r - x)} =$$

$$-\phi_2 = \frac{P_2}{\rho_0 U} e^{\frac{1\omega}{U}(x_r + \epsilon - x)} =$$

$$-\phi_3 = \frac{P_3}{\rho_0 U} e^{\frac{1\omega}{U}(x_r + 2\epsilon - x)} =$$

$$-\phi_4 = \frac{P_4}{\rho_0 U} e^{\frac{1\omega}{U}(x_r + 3\epsilon - x)} =$$

Composite ϕ



$$\phi_{01} = -\frac{\epsilon}{\rho_0 U} \alpha P_1 \quad ; \quad \alpha = e^{-\frac{1\omega\epsilon}{2U}}$$

$$\phi_{02} = -\frac{\epsilon}{\rho_0 U} (\alpha^3 P_1 + \alpha P_2)$$

$$\phi_{03} = -\frac{\epsilon}{\rho_0 U} (\alpha^5 P_1 + \alpha^3 P_2 + \alpha P_3)$$

$$\phi_{04} = -\frac{\epsilon}{\rho_0 U} (\alpha^7 P_1 + \alpha^5 P_2 + \alpha^3 P_3 + \alpha P_4)$$

$$\phi_{05} = -\frac{\epsilon}{\rho_0 U} (\alpha^9 P_1 + \alpha^7 P_2 + \alpha^5 P_3 + \alpha^3 P_4)$$

$$\phi_{0n} = -\frac{\epsilon}{\rho_0 U} (P_1 \alpha^{2n-1} + P_2 \alpha^{2n-3} + P_3 \alpha^{2n-5} + P_4 \alpha^{2n-7})$$

Figure 5. Establishment of "Equivalent" Concentrated Dipoles

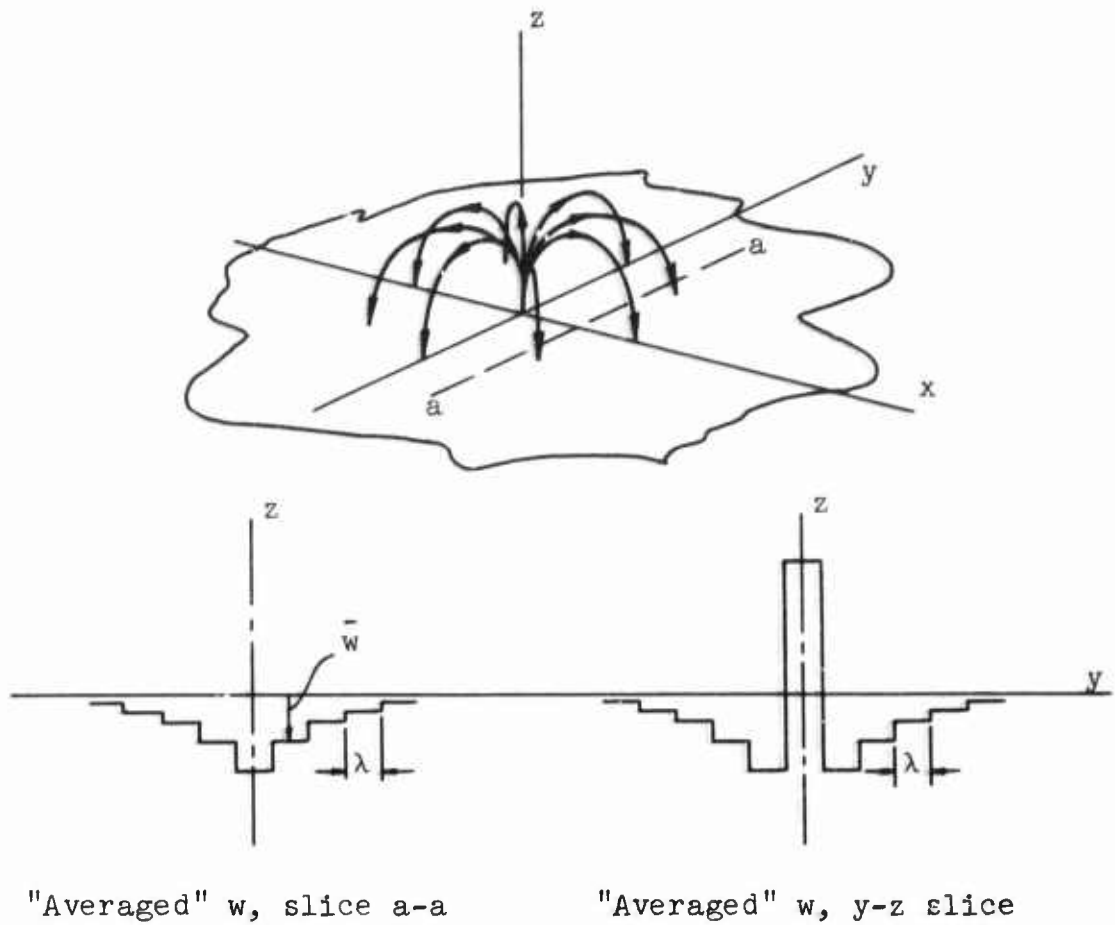


Figure 6. Dipole Representation and "Averaged" Vertical Velocities

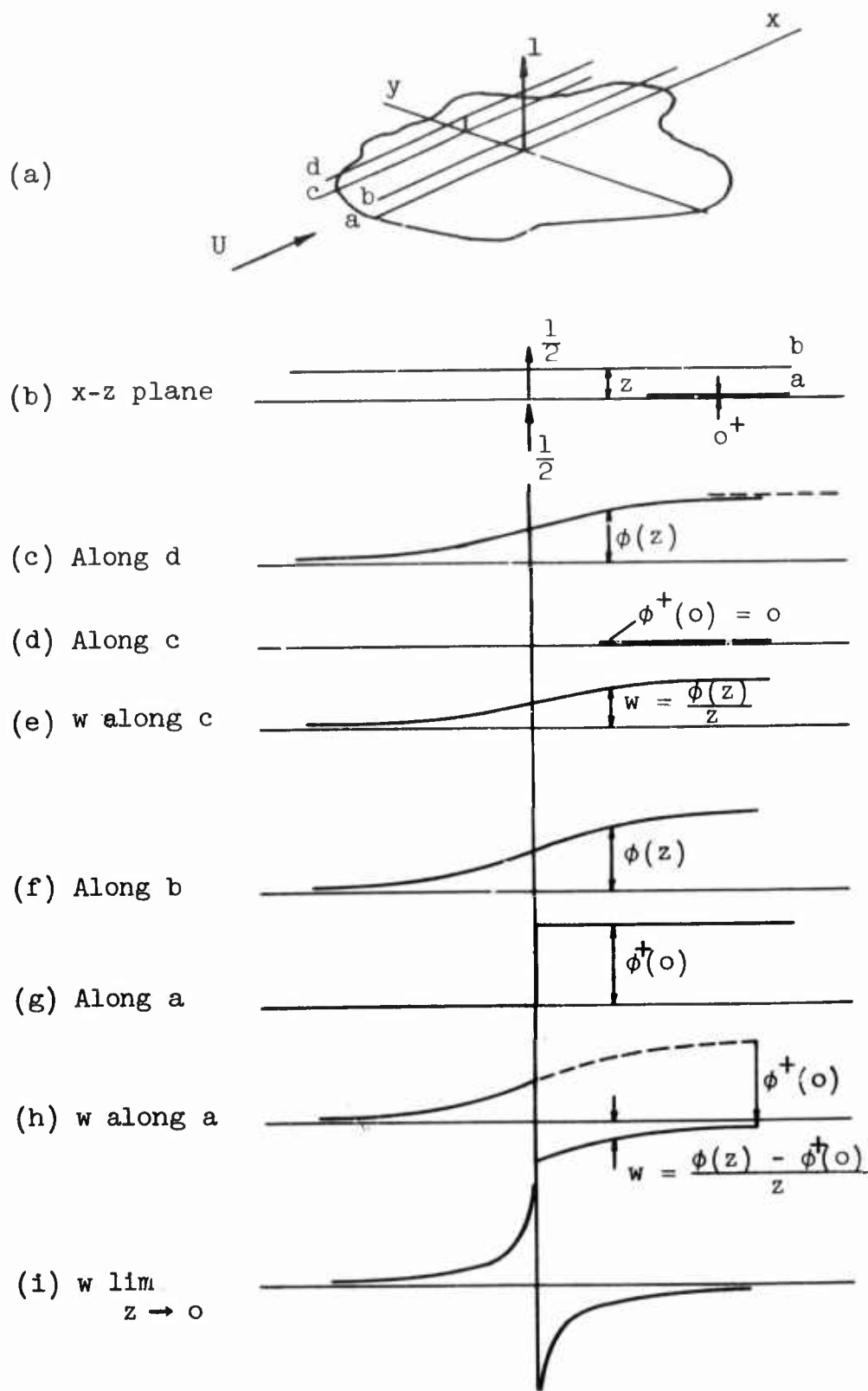
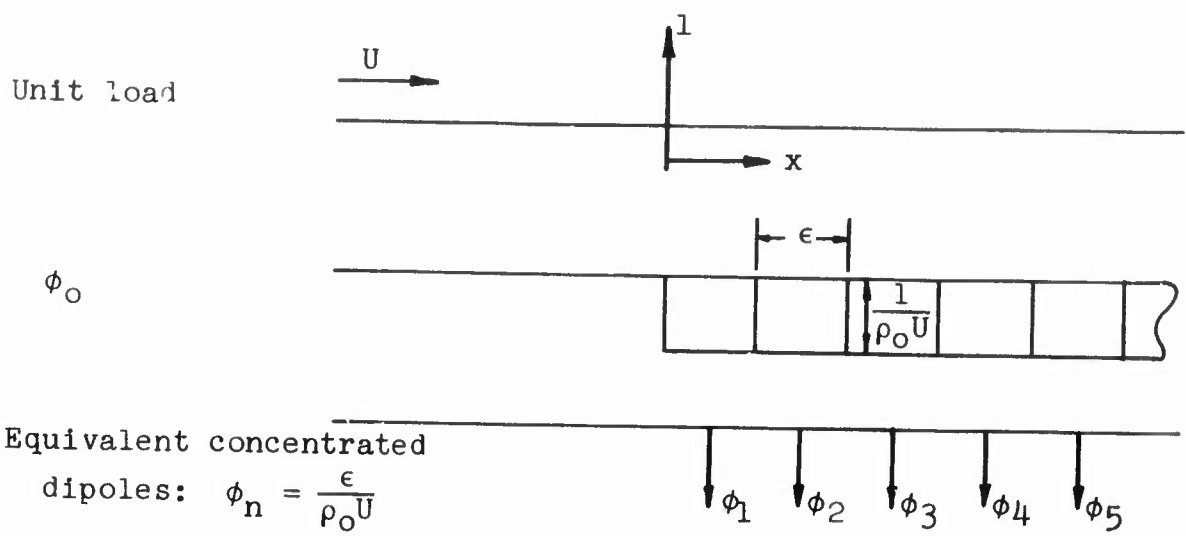


Figure 7. Determination of w by Finite Difference Technique



$\bar{w} = \frac{2}{\pi \rho_0 U \epsilon} \times$	\dots	$\frac{1}{63}$	$\frac{1}{35}$	$\frac{1}{15}$	$\frac{1}{3}$	-1	$\frac{1}{3}$	$\frac{1}{15}$	$\frac{1}{35}$	$\frac{1}{63}$	\dots	
"	"	\dots	$\frac{1}{99}$	$\frac{1}{63}$	$\frac{1}{35}$	$\frac{1}{15}$	$\frac{1}{3}$	-1	$\frac{1}{3}$	$\frac{1}{15}$	$\frac{1}{35}$	\dots
	\dots	\dots	$\frac{1}{43}$	$\frac{1}{99}$	$\frac{1}{63}$	$\frac{1}{35}$	$\frac{1}{15}$	$\frac{1}{3}$	-1	$\frac{1}{3}$	$\frac{1}{15}$	\dots
	\dots	\dots	$\frac{1}{195}$	$\frac{1}{143}$	$\frac{1}{99}$	$\frac{1}{63}$	$\frac{1}{35}$	$\frac{1}{15}$	$\frac{1}{3}$	-1	$\frac{1}{3}$	\dots
	\dots	\dots	\dots	\dots	\dots	\dots	\dots	\dots	\dots	\dots	\dots	\dots
$w = \sum = \frac{2}{\pi \rho_0 U \epsilon} \times$		$\frac{1}{14}$	$\frac{1}{10}$	$\frac{1}{6}$	$\frac{1}{2}$	$-\frac{1}{2}$	$-\frac{1}{6}$	$-\frac{1}{10}$	$-\frac{1}{14}$	$-\frac{1}{18}$		

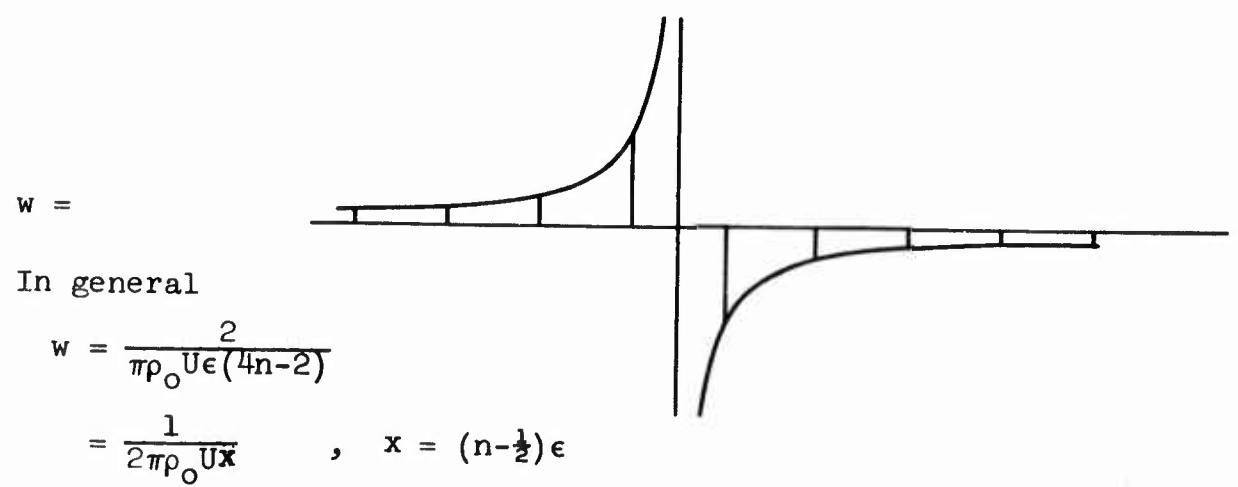


Figure 8. Downwash Due to a Unit Load as Obtained from Wake Dipoles

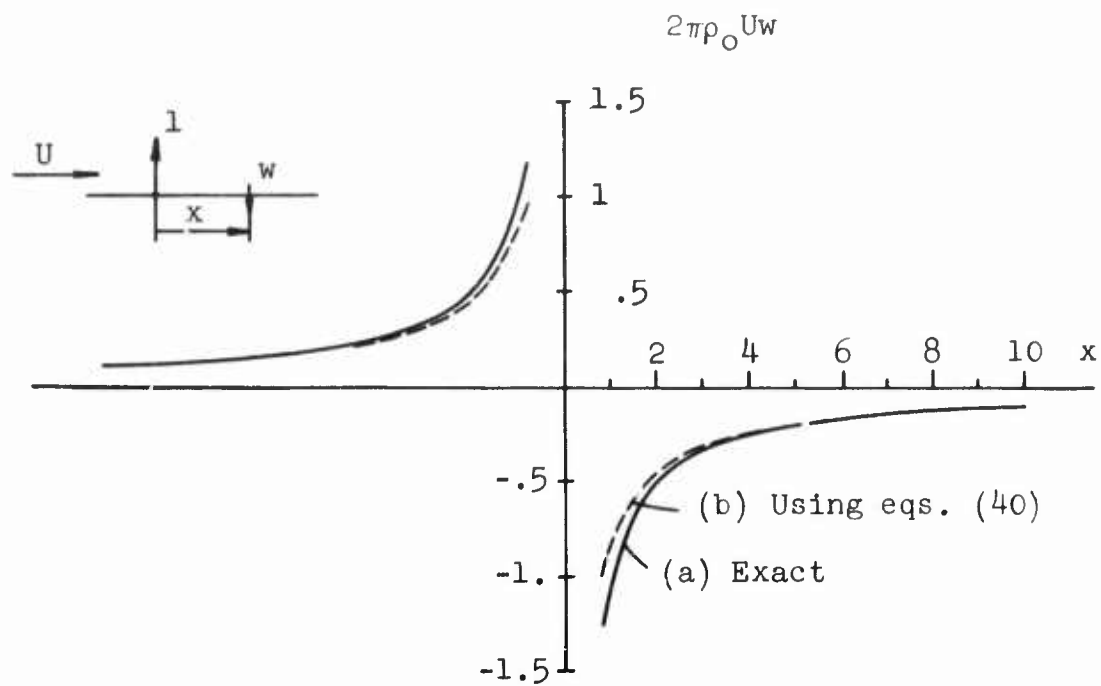


Figure 9. Downwash Values for Solution 3

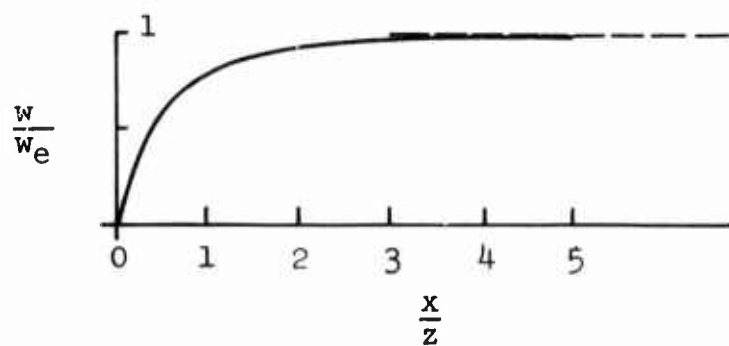


Figure 10. Downwash Solution for Unit Load by Finite - Difference Technique with z Finite

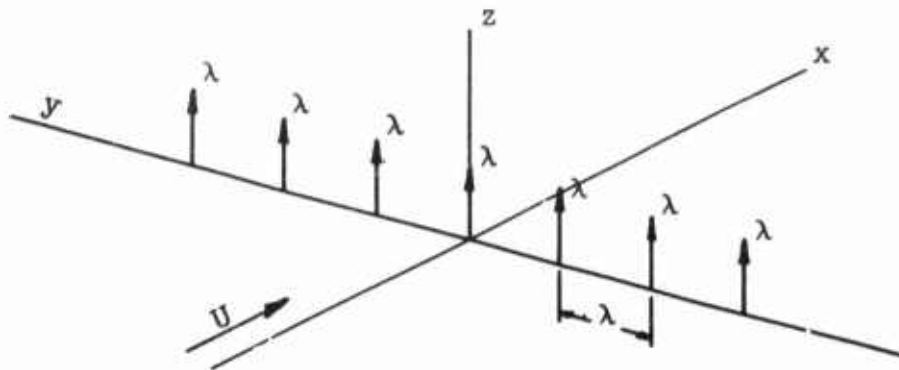


Figure 11. Infinite Array of Equally Spaced Concentrated Loads Replacing a Continuous Line Source

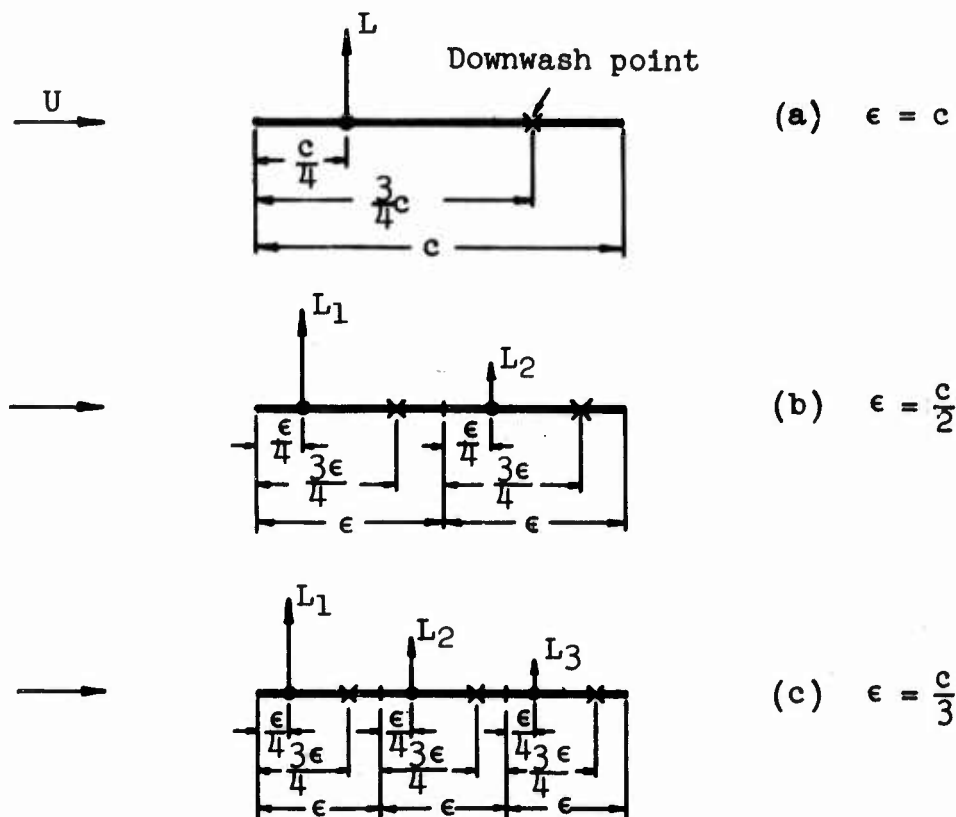


Figure 12. Example Airfoil Cases Treated

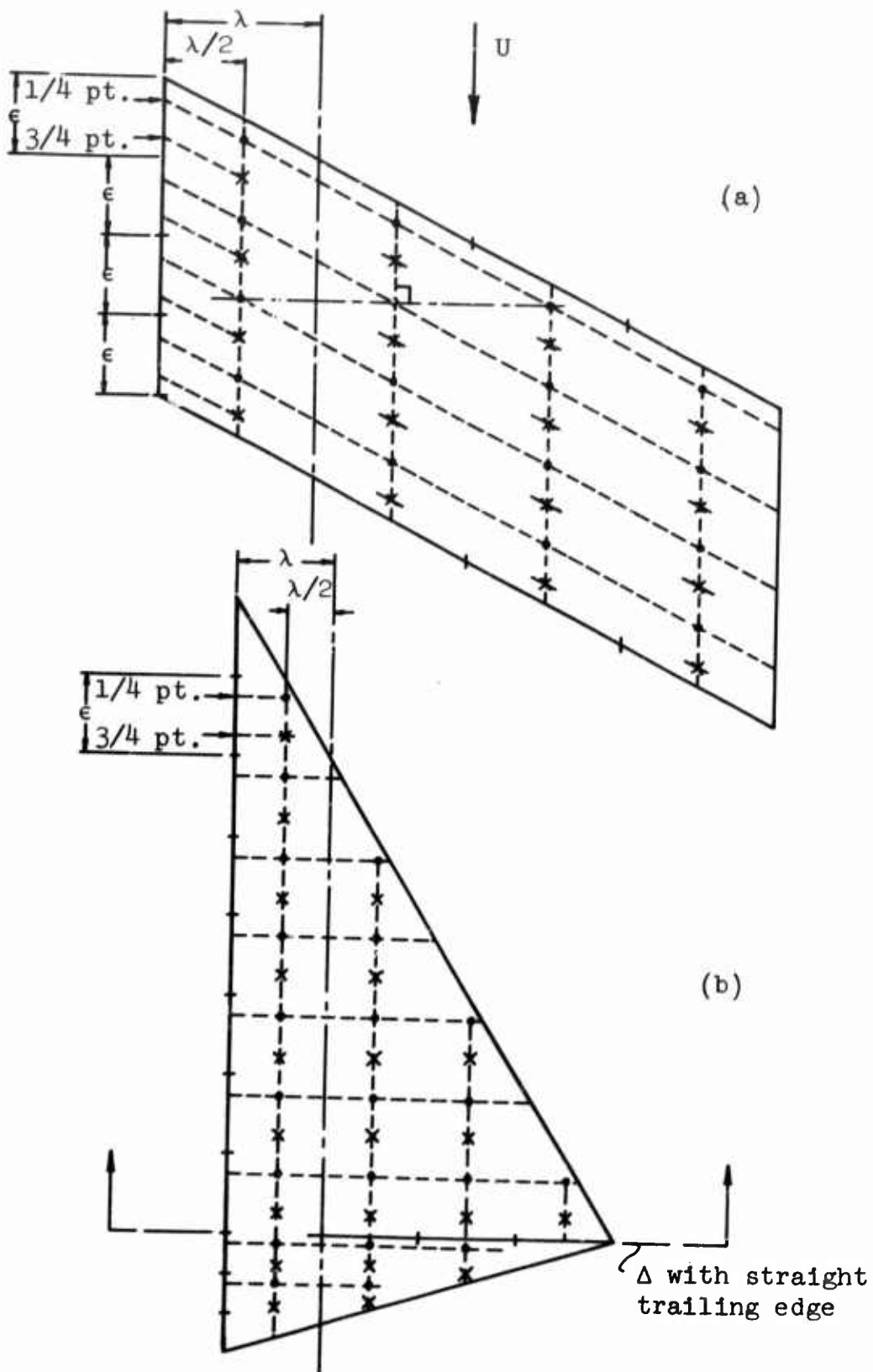
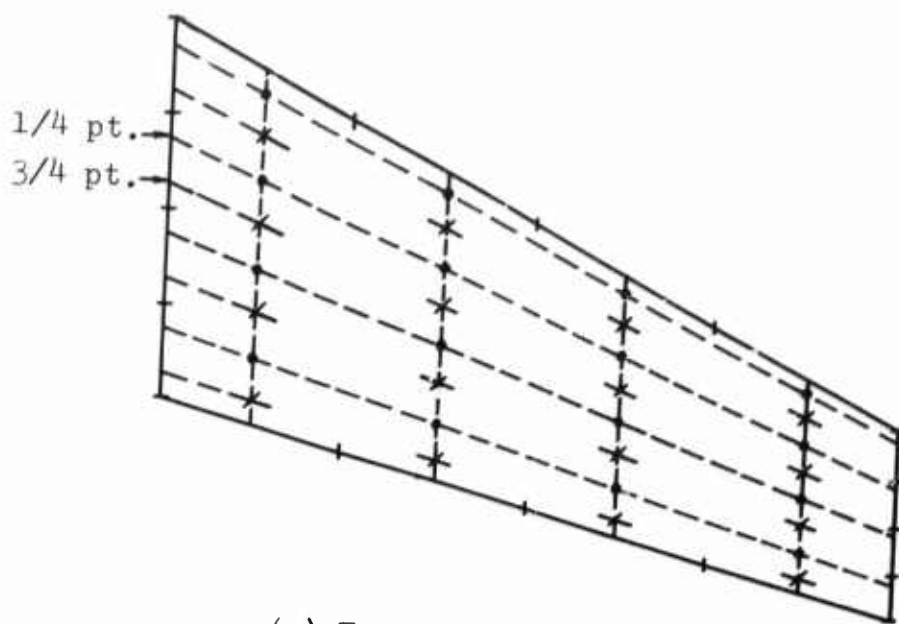
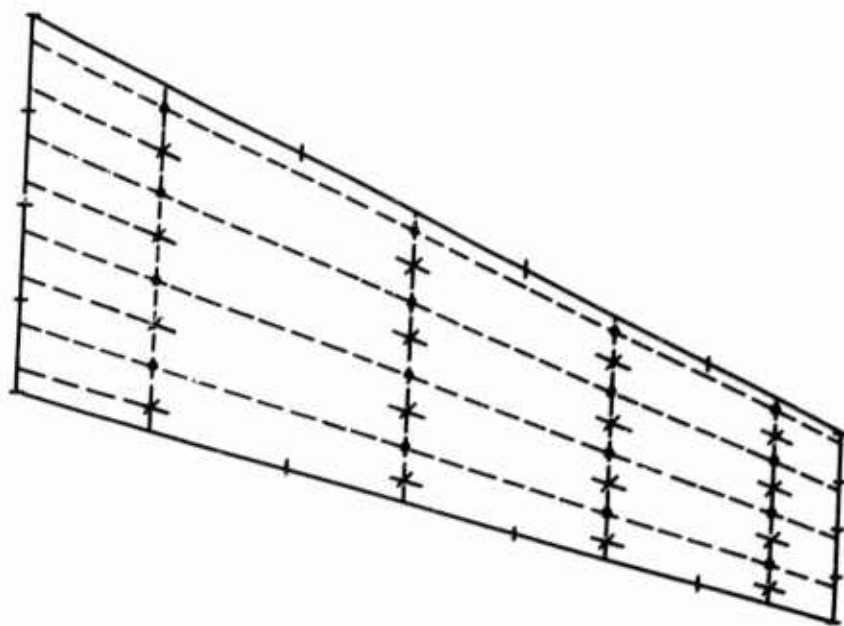


Figure 13. Ideas on Possible Grid Layouts

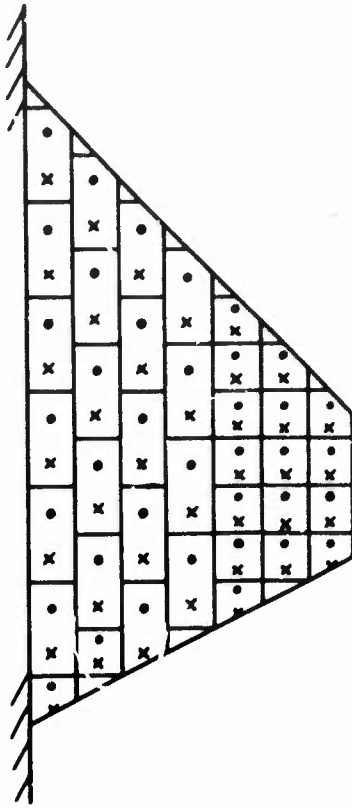


(c) Equal spanwise intervals



(d) Spanwise intervals vary proportional to chord intervals

Figure 13. Cont.



(e) Mixed simple rectangular boxes

Figure 13. Concluded

Unclassified
Security Classification

DOCUMENT CONTROL DATA - R & D		
<i>(Security classification of title, body of abstract and indexing annotation must be entered when the overall report is classified)</i>		
1. ORIGINATING ACTIVITY (Corporate author) Aeronautical Research Associates of Princeton, 50 Washington Road Princeton, New Jersey 08540		2a. REPORT SECURITY CLASSIFICATION Unclassified
		2b. GROUP N/A
3. REPORT TITLE Some New Concepts in Oscillatory Lifting Surface Theory		
4. DESCRIPTIVE NOTES (Type of report and inclusive dates) Final Report; December 1966 - October 1968		
5. AUTHOR(S) (First name, middle initial, last name) John C. Houbolt		
6. REPORT DATE June 1969	7a. TOTAL NO. OF PAGES 68	7b. NO. OF REFS 3
8a. CONTRACT OR GRANT NO. F33615-67-C-1191	8b. ORIGINATOR'S REPORT NUMBER(S) ARAP Report No. 126	
b. PROJECT NO. 1367		
c. Task No. 136702 d. BPSN: 7(61136702-62405334)	9b. OTHER REPORT NO(S) (Any other numbers that may be assigned this report) AFFDL-TR-69-2	
10. DISTRIBUTION STATEMENT This document is subject to special export controls and each transmittal to foreign governments or foreign nationals may be made only with prior approval of the Air Force Flight Dynamics Laboratory (FDTR), Wright-Patterson Air Force Base, Ohio 45433.		
11. SUPPLEMENTARY NOTES	12. SPONSORING MILITARY ACTIVITY Air Force Flight Dynamics Laboratory Air Force Systems Command, USAF	
13. ABSTRACT <p>New developments on lifting surface theory for oscillatory subsonic flow are given. Key concepts in the analysis are the use of concentrated loads rather than distributed pressure "mode" shapes, and the development of a modified kernel function which gives average values of vertical velocity over chosen intervals and which eliminates all singularity problems.</p> <p>Features of the analysis are (1) loads are given directly in terms of vertical velocities, (2) no pressure modes have to be assumed, (3) singularities are obviated, (4) the locations of control downwash points are specified systematically, (5) control surfaces may be included, (6) treatment of nonplanar surfaces, such as T-tails, is possible, and (7) application is made through a simple quick routine procedure. Examples are given throughout to illustrate the concepts.</p> <p>This abstract is subject to special export controls, and each transmittal to foreign governments or foreign nationals may be made only with prior approval of the Air Force Flight Dynamics Laboratory (FDTR), Wright-Patterson Air Force Base, Ohio 45433.</p>		

DD FORM 1473
1 NOV 65

Unclassified
Security Classification

14. KEY WORDS	LINK A		LINK B		LINK C	
	ROLE	WT	ROLE	WT	ROLE	WT
Oscillatory air flow						
Nonsteady						
Subsonic						
Kernel function						
Lifting surface theory						
Finite wings						
Nonplanar surfaces						
Frequency response						